Titre: Title:	Modeling Radiofrequency Heating of Embolization Coils for the Treatment of Cerebral Aneurysm
Auteur: Author:	Pariya Salami
Date:	2010
Type:	Mémoire ou thèse / Dissertation or Thesis
Référence: Citation:	Salami, P. (2010). Modeling Radiofrequency Heating of Embolization Coils for the Treatment of Cerebral Aneurysm [Mémoire de maîtrise, École Polytechnique de Montréal]. PolyPublie. https://publications.polymtl.ca/380/

URL de PolyPublie: PolyPublie URL:	https://publications.polymtl.ca/380/
Directeurs de recherche: Advisors:	Pierre Savard, & Jean Raymond
Programme: Program:	Génie biomédical

UNIVERSITÉ DE MONTRÉAL

MODELING RADIOFREQUENCY HEATING OF EMBOLIZATION COILS FOR THE TREATMENT OF CEREBRAL ANEURYSM

PARIYA SALAMI
INSTITUT DE GÉNIE BIOMÉDICAL
ÉCOLE POLYTECHNIQUE DE MONTRÉAL

MÉMOIRE
PRÉSENTÉ EN VUE DE L'OBTENTION
DU DIPLÔME DE MAÎTRISE ÈS SCIENCES APPLIQUÉES
(GÉNIE BIOMÉDICAL)
Août 2010

UNIVERSITÉ DE MONTRÉAL

ÉCOLE POLYTECHNIQUE DE MONTRÉAL

Ce mémoire intitulé:

MODELING RADIOFREQUENCY HEATING OF EMBOLIZATION COILS FOR THE TREATMENT OF CEREBRAL ANEURYSM

présenté par : SALAMI Pariya
en vue de l'obtention du diplôme de : Maitrise ès sciences appliquées
a été dûment accepté par le jury d'examen constitué de :

M. LESAGE, Frédéric, Ph.D., président
M. SAVARD, Pierre, Ph.D., membre et directeur de recherche
M. RAYMOND, Jean, M.D., membre et codirecteur de recherche
M. BERTRAND, Michel, Ph.D., membre

ACKNOWLEDGMENTS

I would like to take this opportunity to thank the people who helped me accomplish the goals of my research.

First of all, I would like to express my deepest gratitude to my supervisor, Dr. Pierre Savard, for his great mentorship and guidance. He was very kind and supportive in many ways.

I also want to thank my co-supervisor Dr. Jean Raymond for his guidance in this area and his valuable advice.

I am indeed thankful to the professors and my colleagues at 'École Polytechnique de Montréal' for their support and amity to pursue a graduate degree and complete this research.

My special acknowledgment goes to all my dear friends for their support and kindness.

And last, but certainly not least, I will always be grateful to my parents, my brother and my beloved grandfather for their sincere love and support.

RÉSUMÉ

L’anévrisme intracrânien est une déformation de la paroi d'une artère du cerveau qui provoque une dilatation localisée du vaisseau sanguin. Les anévrismes non traités peuvent se déchirer et causer une hémorragie sous-arachnoïdienne (SAH) et, dans certains cas, des accidents vasculaires cérébraux.

Les traitements courants sont la chirurgie et les traitements endovasculaires. Le traitement endovasculaire le plus populaire est l'embolisation à l'aide de spirales qui a été proposée par G. Guglielmi en 1991 (ces spirales sont des endoprothèses vasculaires ayant la forme arrondie d'un ressort). Cette méthode, qui est actuellement utilisée pour traiter environ 80% des anévrismes cérébraux, consiste à insérer un cathéter dans l'aorte, puis à le guider vers le vaisseau désiré de façon à insérer des spirales de platine à l'intérieur de l'anévrisme. Ces spirales induisent une coagulation puis l’obstruction de l’anévrysme. Un problème possible est que l'anévrisme ainsi traité peut se recanaliser après quelques mois pour des raisons inconnues. Bien que les mécanismes de la recanalisation demeurent incertains, l'une des hypothèses est que celle-ci provient de l'endothélium et que la dénudation endothéliale pourrait prévenir cette recanalisation. Certaines méthodes de dénudation endothéliales ont déjà été étudiées, telles que l'abrasion mécanique avec le dispositif col-pont anévrismal (*aneurismal neck-bridge device*, ANBD) et la cryoablation. Ces deux méthodes ont toutefois présenté des résultats non désirés. La nouvelle méthode qui est étudiée dans ce mémoire est l'ablation thermique par courant radiofréquence (*radiofrequency ablation*, RFA).

À la suite d’études préliminaires *in vivo*, il semble que la résection par courant radiofréquence puisse être efficace pour la dénudation endothéliale et l’amélioration de l'embolisation par spirales. Le principal objectif de notre projet est d’étudier les effets du courant radiofréquence appliqué directement ou au voisinage d’une spirale endovasculaire sur la distribution de température des tissus environnants pour optimiser le processus de livraison d'énergie. Pour atteindre cet objectif, les caractéristiques inductives et résistives des spirales, ainsi que les effets

de la longueur et la forme de la sonde sur la distribution de la température ont été étudiés en utilisant une approche par modélisation numérique. Des expériences *in vitro* ont également été effectuées afin de valider les simulations par ordinateur.

En conclusion, nous suggérons que le courant de radiofréquence ne doit pas être injecté directement aux spirales de platine à cause de leur grande résistance électrique, mais qu'il doit être injecté dans un applicateur en acier placé au centre des spirales. Aussi, un applicateur d'une longueur de 6 à 10 mm est approprié pour générer des distributions uniformes de température. Enfin, des études animales devraient être réalisées afin d'étudier davantage cette approche prometteuse.

ABSTRACT

Cerebral aneurysm is a weakness in the wall of a cerebral artery which causes a localized dilation or ballooning of the blood vessel. Untreated aneurysms in the brain may rupture and cause subarachnoid hemorrhage (SAH) and in some cases, stroke.

Treatment may be surgical or endovascular treatments. The most popular endovascular treatment is coil embolization, first introduced with controlled detachment by G. Guglielmi in 1991. This method, which is currently used to treat approximately 80% of cerebral aneurysms, consists in inserting a catheter in the aorta and then guiding it to the desired region of the cerebral vasculature to insert small platinum coils inside the aneurysm. These coils induce clotting and occlude the aneurysms. A possible problem is that the occluded aneurysm can be recanalized after some months because of unknown reasons. Though the exact mechanism responsible for recanalization remains unclear, one of the hypotheses is that recanalization is related to the endothelium and that endothelial denudation can prevent recanalization. Some methods of denudation have been previously investigated, such as mechanical abrasion with the aneurismal neck-bridge device (ANBD) and cryoablation. Both methods showed undesirable results. The new method which is investigated in this memoir is radiofrequency ablation (RFA).

Based on preliminary *in vivo* studies, it is believed that RFA can be effective in endothelial denudation and in improving the results of coil embolization. The main objective of our project is to investigate the effects of radiofrequency current applied to an endovascular platinum coil on the temperature distribution of perianeurysmal tissues so as to optimize the energy delivery process. To achieve this goal, inductive and resistive characteristics of the embolization coils, as well as the effects of the length and shape of the electrode on the temperature distribution was investigated using a computer modeling approach. *In vitro* experiments were also performed to validate the computer simulations.

Based on this study, we conclude that platinum coils should not be used for the direct application of RF current. A steel applicator placed in the center of the endovascular coils is more

appropriate. Also, an applicator length of 6 to 10 mm is optimized for generation of a uniform temperature distribution. Finally, animal studies should be performed to further investigate this promising approach.

CONDENSÉ EN FRANÇAIS

L’anévrisme cérébral

L’anévrisme cérébral est une déformation de la paroi d'une artère du cerveau qui provoque une dilatation localisée du vaisseau sanguin.

Dans la plupart des cas, les anévrismes sont asymptomatiques et ils sont habituellement découverts durant l’imagerie cérébrale utilisée pour investiguer l’origine de symptômes non-associés à l’anévrisme comme des maux de tête, des étourdissements, des douleurs aux yeux et des problèmes de vision.

Si un anévrisme n’est pas détecté, il peut se rompre et causer une hémorragie sous-arachnoïdienne, et dans certains cas, des accidents vasculaires cérébraux ou la mort. La taille et la position de l’anévrisme sont des facteurs de risque pour l’hémorragie.

Lorsqu’un vaisseau sanguin se rompt, le sang se répand et le cerveau doit alors faire face à de sérieux problèmes: les tissus ne reçoivent plus suffisamment d’oxygène et de nutriments, la pression augmente et les tissus enflent.

Environ 20% des accidents vasculaires cérébraux se déroulent de cette façon. Parfois, des symptômes comme des maux de tête, des nausées, des raidissements du dos ou des jambes peuvent durer durant plusieurs jours.

Toutefois, lorsque l’anévrisme se rompt soudainement, les symptômes précédents peuvent être plus sévères, auxquels peuvent s’ajouter de l’hypertension, des pertes d’équilibre, une vision floue, de la photophobie, de l’irritabilité, de l’inconscience et même un coma profond.

Prévalence et incidence de l’anévrisme cérébral

Des études ont montré que la prévalence des anévrismes cérébraux dans la population adulte varie de 1% à 5%. L’incidence est plus élevée de la fin de la quarantaine jusqu’au début de la soixantaine. L’incidence est plus élevée chez les femmes que chez les hommes. L’incidence d’hémorragie sous-arachnoïdienne due à une rupture d’anévrisme cérébral est d’environ un cas par 10,000 personnes chaque année aux États-Unis.

Les différentes modalités de traitement de l’anévrisme cérébral

Les traitements les plus courants sont l’observation (traitement conservateur), la chirurgie et les traitements endovasculaires.

Le choix du traitement dépend de facteurs tels que la forme, la taille et la position de l’anévrisme; l’âge du patient, son état de santé général, son histoire médicale, les symptômes, la présence ou l’absence de facteurs de risque pour la rupture de l’anévrisme, l’opinion et les préférences du patient. Toutes ces conditions peuvent influencer le résultat du traitement.

Le traitement chirurgical est la plus ancienne modalité de traitement. Toutefois, il est de moins en moins utilisé à cause de l’apparition de techniques beaucoup moins effractives comme le traitement endovasculaire.

Le traitement endovasculaire le plus populaire est l'embolisation de spirales qui a été proposée par G. Guglielmi en 1991 (ces spirales sont des endoprothèses vasculaires ayant la forme arrondie d'un ressort très mince).

Cette méthode, qui est actuellement utilisée pour traiter environ 80% des anévrismes cérébraux, consiste à insérer un cathéter dans l'aorte, puis à le guider vers le vaisseau désiré de façon à

insérer des spirales de platine à l'intérieur de l'anévrisme. Ces spirales induisent une coagulation puis l'obstruction de l'anévrisme.

Problèmes de recanalisation de l'anévrisme cérébral après traitement avec spirales

Un problème possible avec cette méthode est que l'anévrisme ainsi traité peut se recanaliser après quelques mois pour des raisons inconnues. Bien que les mécanismes de la recanalisation demeurent incertains, l'une des hypothèses est que celle-ci provient de l'endothélium et que la dénudation endothéliale pourrait prévenir cette recanalisation.

Certaines méthodes de dénudation endothéliales ont déjà été étudiées, telles que l'abrasion mécanique avec le dispositif col-pont anévrismal (*aneurismal neck-bridge device*, ANBD) et la cryoablation. Ces deux méthodes ont toutefois présenté des résultats non désirés.

La nouvelle méthode qui est étudiée dans ce mémoire est la résection par courant radiofréquence (*radiofrequency ablation*), qui a été suggérée par J. Raymond.

Objectif du projet de recherche

À la suite d'études préliminaires *in vivo,* il semble que la résection par courant radiofréquence puisse être efficace pour la dénudation endothéliale et l'amélioration de l'embolisation des spirales.

Le principal objectif de notre projet est d'étudier les effets du courant radiofréquence appliqué directement ou au voisinage d'une spirale endovasculaire sur la distribution de température du tissu cérébral pour optimiser le processus de livraison d'énergie.

Pour atteindre cet objectif, les caractéristiques inductives et résistives des spirales, ainsi que les effets de la longueur et la forme de la sonde sur la distribution de la température ont été étudiés

en utilisant une approche par modélisation numérique. Des expériences *in vitro* ont également été effectuées afin de valider les simulations par ordinateur.

Absence d'effets fréquentiels

Avant de construire des modèles numériques, nous devons déterminer si la distribution du courant dépend de sa fréquence.

Les études préliminaires sur la résection par courant radiofréquence ont montré que la température n'est pas répartie uniformément autour de la spirale. Une explication possible de ce phénomène est que l'enroulement hélicoïdal du conducteur de platine produit une charge inductive qui bloque de plus en plus le passage du courant radiofréquence tout au long de la spirale.

Selon cette hypothèse, cet effet devrait s'accentuer pour des fréquences plus élevées et s'atténuer pour des fréquences plus faibles.

Afin de tester cette hypothèse, une première série d'expériences *in vitro* fut réalisée en appliquant un courant radiofréquence à une spirale plongée dans un gel électrolytique et en mesurant la distribution de température du gel à différents moments.

Le modèle se composait d'une spirale de platine placée dans une boîte de Pétri de 9 cm de diamètre, remplie d'un gel électrolytique de conductivité électrique similaire à celle des liquides organiques (0,67 $S.m^{-1}$) et ayant une épaisseur de 3 mm.

Une bande métallique circulaire de 8 cm de diamètre fut placée dans la boîte de Pétri comme électrode de retour pour compléter le circuit. Un courant RF de différentes fréquences (50 à 5000 kHz) et différentes amplitudes (100 à 700 mV) fut appliqué à l'extrémité de la spirale.

Les tensions et la température ont été mesurées à l'aide d'un oscilloscope et d'un thermomètre, respectivement. Pour observer la distribution de température, une mince pellicule sensible à la température fut placée dans la boîte de Pétri.

Les résultats de ces expériences ont montré que la distribution de la température n'était pas modifiée lorsque la fréquence changeait.

Mesure de l'impédance des spirales

Pour poursuivre l'évaluation des effets inductifs et résistifs des spirales, les impédances résistives et inductives de différents types de spirales furent mesurées à différentes fréquences (50, 500 et 5000 kHz).

Les résultats de cette étude ont montré que l'impédance des différentes spirales reste presque constante malgré l'augmentation de la fréquence, mais que les impédances résistives de tous les types de spirales étaient beaucoup plus élevées que les impédances inductives.

Ce résultat indique que la baisse de la température qui a été précédemment observée sur toute la longueur de la spirale n'est pas due à des effets inductifs, mais est due à la baisse de potentiel produite par la résistance élevée de la spirale.

Ceci suggère également que le courant radiofréquence ne devrait pas être appliqué directement à une extrémité de la spirale, mais à un applicateur de faible résistance placé à l'intérieur de la spirale pour avoir une distribution plus homogène de la température.

Modélisation du potentiel et de la température par la méthode des éléments finis

Les distributions de courant et de potentiel ne dépendant pas de la fréquence, tel que déterminé précédemment, ces distributions peuvent être calculées en résolvant l'équation de Laplace.

Plusieurs modèles numériques de spirales et d'applicateurs incorporés dans des milieux conducteurs représentant le tissu cérébral furent ainsi créés à l'aide du logiciel COMSOL® Multiphysics 3.5a.

La méthode des éléments finis fut utilisée pour calculer d'abord la distribution du courant; par la suite, la densité de puissance dissipée par ce courant dans le tissu fut utilisée pour calculer l'évolution temporelle de la distribution de la température.

Modèle de spirale à résistance élevée

Le premier modèle consiste en une forme cylindrique mince de 2 cm de long représentant une spirale de platine de résistance élevée, immergée dans une autre forme cylindrique aplatie représentant la boîte de Pétri.

Ce modèle a confirmé les résultats des études préliminaires, soit que la température n'est pas répartie uniformément sur toute la longueur de la spirale et qu'elle est plus élevée au point d'entrée du courant, au début de la spirale.

Modèle d'applicateur à résistance faible : optimisation des dimensions

Le second modèle possède une géométrie de base semblable à celle du premier, sauf que la résistance du petit cylindre est beaucoup plus faible de façon à représenter un applicateur en acier plutôt qu'une spirale de platine de résistance élevée.

Après avoir montré que la puissance dissipée ne s'atténue pas le long de l'applicateur à cause de sa résistance faible, la géométrie de l'applicateur fut modifiée pour trouver la taille optimale pour produire une distribution de température uniforme. Les dimensions suivantes de l'applicateur furent étudiées, rayon : 100 μm, 150 μm et 200 μm ; et longueur : 3 mm, 6 mm, 10 mm, 15 mm et 20 mm.

Les résultats ont montré que: la température maximum du tissu est plus élevée pour les applicateurs courts et minces; qu'une augmentation de température était observée aux deux extrémités des applicateurs longs ; et que pour produire une distribution de température uniforme, des applicateurs avec un rayon de 200 μm et une longueur comprise entre 6 mm et 10 mm étaient les plus appropriés.

Modèle d'applicateur inséré dans une spirale

Un troisième modèle constitué d'un applicateur d'acier semblable à celui du modèle précédent disposé dans l'axe d'un solénoïde de platine représentant une spirale endovasculaire fut construit pour étudier l'influence de la spirale de platine sur la distribution de température. La tension fut appliquée à une extrémité de l'applicateur et non pas à la spirale directement.

L'addition de la spirale de platine n'a produit qu'un très faible changement de la température maximale du tissu, et pratiquement aucun changement dans la distribution de température autour des spirales. Ces simulations démontrent l'efficacité de l'injection du courant radiofréquence à un applicateur en acier plutôt qu'à une spirale de platine.

Étude de validation de la résolution du maillage

Tous les modèles à éléments finis précédents furent également résolus avec un plus grand nombre d'éléments pour vérifier s'il y a un changement significatif dans les résultats. Le maillage fut ainsi affiné à quatre reprises pour le modèle d'applicateur en acier et le modèle d'applicateur au centre de la spirale de platine.

Il fut observé que pour les applicateurs très petits, des mailles plus fines mènent à un résultat plus précis et améliorent le résultat, mais que pour les applicateurs plus grands qui sont l'objet principal de notre étude, il n'a pas d'effets significatifs.

Modèle d’applicateur inséré dans une spirale : expériences additionnelles

Pour valider certains des résultats de simulation par des expériences *in vitro,* un applicateur avec un diamètre de 0.46 mm fut placé dans la boîte de Pétri, et la distribution de température fut mesurée en appliquant un courant radiofréquence à 500 kHz pour des longueurs différentes de l'applicateur (3 mm, 6 mm, 10 mm, 15 mm et 20 mm).

De plus, pour confirmer les résultats en présence de la spirale de platine, l’expérience fut reprise en plaçant le même applicateur au centre d'une spirale de platine ayant les caractéristiques suivantes: longueur de 8 mm, rayon de 2 mm, rayon de la section transversale de 0,19 mm. La longueur de l'applicateur en acier fut changée comme précédemment.

Puisque dans les modèles informatiques précédents le calibre de l'applicateur ne correspond pas à celui de cette dernière étude expérimentale, de nouveaux modèles numériques avec des dimensions et des caractéristiques identiques aux expériences furent créés.

Les résultats de ces expériences ont coïncidé avec ceux des simulations pour ce qui est de la forme des distributions de température, toutefois, les températures maximales mesurées étaient plus faibles que les températures simulées, peut être à cause de la taille du capteur de température et de l’effet de l’exposition à l‘air de la préparation expérimentale.

Modèle de volume conducteur semblable au cerveau

Des simulations furent effectuées dans un modèle présentant une géométrie plus proche de celle du cerveau. Ce modèle se compose d'un grand cylindre (avec un diamètre et une hauteur de 8 cm), représentant le cerveau et d’un petit cylindre au centre avec les caractéristiques de l'applicateur en acier.

Les simulations furent effectuées avec deux longueurs optimisées d'applicateur (6 mm et 10 mm) ayant un diamètre de 0.46 mm pour trouver les meilleures tensions et durées d'application et valider la sécurité de la méthode.

Des tensions différentes (5, 10, 15 V) furent appliqués à une extrémité de l'applicateur durant 120 secondes et il a été constaté que pour minimiser les dommages aux tissus nerveux, nous devons prendre en compte la durée d'application et la tension.

Étude des effets de l'augmentation de la conductivité électrique due à la température

Finalement, comme la valeur de la conductivité électrique augmente légèrement avec la température (environ 2% par degré centigrade), le modèle numérique fut modifié pour tenir compte de cet effet et des simulations furent effectuées afin d'évaluer si la conductivité électrique peut être considérée comme constante (comme dans nos simulations précédentes), ou si sa variabilité en fonction de la température ne peut être négligée.

Cette étude a montré que pour des voltages faibles, où la température ne montre pas une grande élévation après 120 secondes, l'influence de la température sur conductivité électrique être négligée. Toutefois, pour des tensions de plus de 15 V, cet effet ne peut être ignoré et il doit être pris en compte.

Conclusion

En conclusion, nous suggérons que le courant de radiofréquence ne doit pas être injecté directement aux spirales de platine à cause de leur grande résistance électrique, mais qu'il doit être injecté dans un applicateur en acier placé au centre des spirales.

Aussi, un applicateur d'une longueur de 6 à 10 mm est approprié pour générer des distributions uniformes de température.

Enfin, des études animales devraient être réalisées afin d'étudier davantage cette approche prometteuse.

TABLE OF CONTENTS

LIST OF TABLES

LIST OF FIGURES

LIST OF ACRONYMS AND ABREVIATIONS

ANBD	Aneurysmal neck-bridge device
AVM	Arteriovenous malformation
BPM	Bioabsorbable Polymeric Material
EVAL	Ethylene Vinyl Alcohol Copolymer
EVT	Endovascular treatment
GDC	Guglielmi detachable coils
ISAT	International subarachnoid aneurysm trial
Lipiodol	Iodized oil
NBCA	N-butyl-2-cyanoacrylate
PVA	Polyvinyl Alcohol
RF	Radiofrequency
RFA	Radiofrequency ablation
SAH	Subarachnoid hemorrhage
SMC	Smooth muscle cells
WSS	Wall shear stress

CHAPTER 1. INTRODUCTION

1.1 Cerebral Aneurysms

In general, arteries have three layers: the tunica externa (mainly composed of connective tissue), the tunica media (smooth muscle cells (SMCs), and elastin) and the tunica intima (endothelial cells; usually 1-3 layers of SMCs). The internal cavity, where blood flows, is called the lumen. The loss or absence of the muscular wall of the artery and of the elastin, which can occur in any blood vessel but more often in arteries than veins, will cause a weakening of the artery. This kind of structural effect may result in a ballooning or widening of the artery which is called a brain aneurysm, cerebral aneurysm, or intracranial aneurysm. Figure 1.1 shows the location of the arteries that are more likely to have aneurysms, along with their prevalence (as published by Brisman (2009)).

There are three types of cerebral aneurysm: saccular, fusiform, and dissecting. The saccular aneurysm, the most common type occurring in 90% of aneurysms, is a “berry” like aneurysm with a narrow stem (or neck). A fusiform aneurysm is a swelling on all sides and is associated with atherosclerosis. A dissecting aneurysm, a less common aneurysm, usually results from a small tear in the inner layer of the arterial wall, with blood entering and separating the structural layers of the artery (Brisman, 2009; Yale Medical Group, 2010). (Figure 1.2)

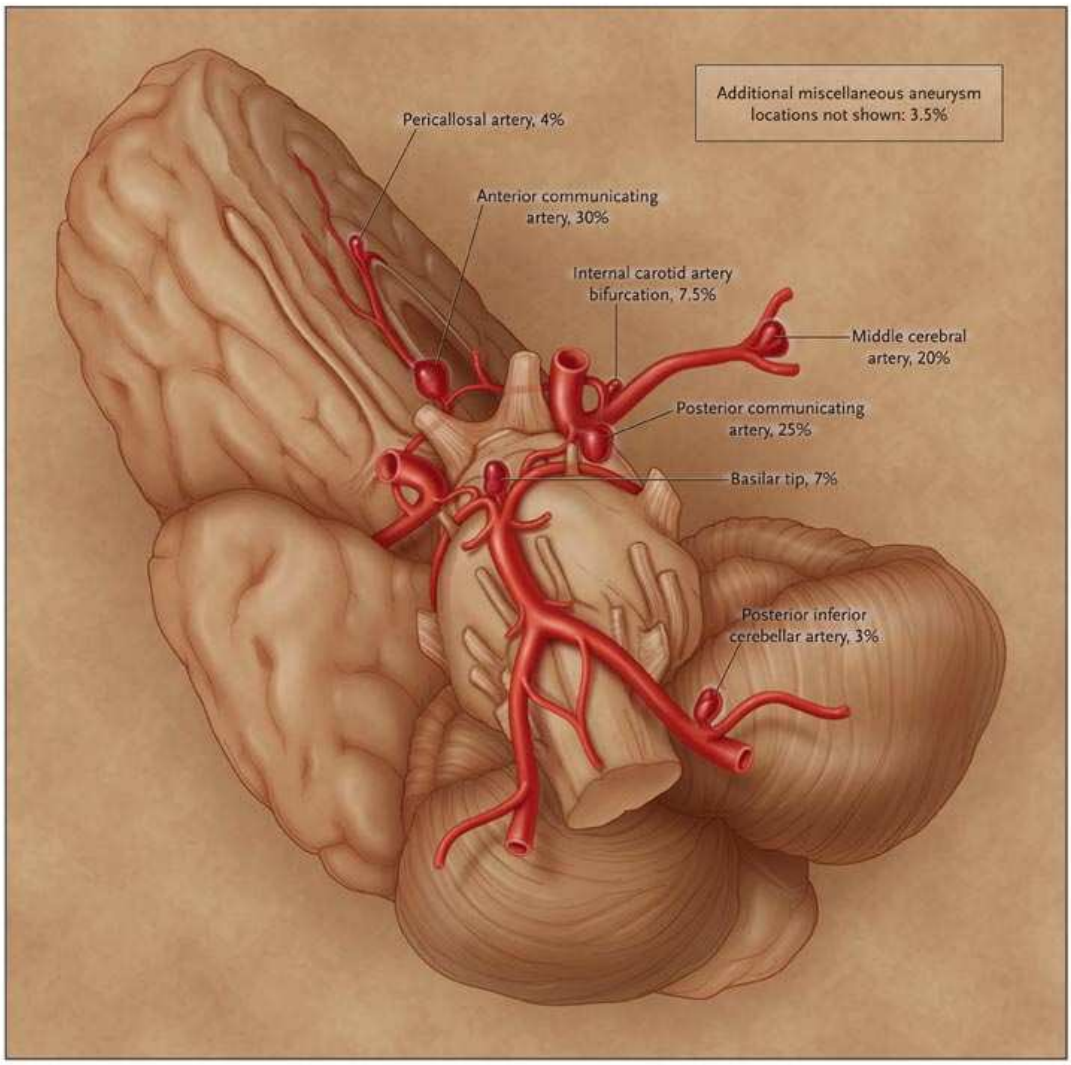

Figure 1.1 Location of the arteries likely to have aneurysm (Brisman, 2009)

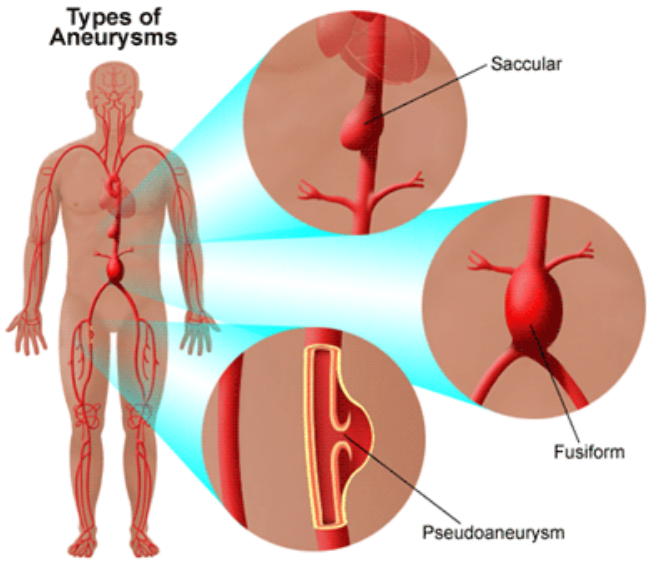

Figure 1.2 Different types of aneurysm (Yale Medical Group, 2010)

1.2 Causes, Developments and Risk Factors

Cerebral aneurysm may have a congenital cause or may be acquired. The frequent localization of saccular aneurysms in cerebral arteries, as compared to other systemic arteries, suggests that, some local factor is involved. Branching patterns may influence the formation of aneurysms. It has been shown that changes in the configuration of the bifurcation could alter blood flow patterns (N. Brown, 1991). Since cerebral aneurysms frequently occur at a vascular branching point or a curvature, its development may depend on various properties of blood flow. For instance hypertension and atherosclerosis can alter the blood flow and this may cause a weakness in the arterial wall (Shojima et al., 2005; Brisman, 2009). Flow may act through two directionally different forces. The first factor is the “impacting force”, acting perpendicular to the vessel wall. The other factor thought to have effects on the creation and development of cerebral aneurysms, is wall shear stress (WSS). WSS is a hemodynamic stress which acts parallel to the vessel wall and affects the cellular function of the endothelium (Shojima et al., 2005; Shojima et al., 2004).

Some congenital risk factors for cerebral aneurysms include arteriovenous malformation (AVM), coarctation of the aorta, polycystic kidney disease, Noonan's syndrome (genetic disorder causing abnormal developments of parts of the body) and many others (Liebeskind, 2009; University of Virginia Health Center, 2007). A familial form may be present in 10% of cases.
Acquired risk factors can be age (>40), hypertension, atherosclerosis, smoking, illicit drug usage, trauma, and infection (Taylor et al., 1995; Brisman, 2009).

1.3 Symptoms

In many cases, cerebral aneurysms remain clinically silent and unruptured aneurysms are discovered during imaging for unrelated symptoms, although it is possible to list headache, dizziness, eye pain, and vision problems as symptoms associated with the discovery of unruptured aneurysms.
Most aneurysms are discovered at the time of ruptures that have caused subarachnoid hemorrhage (SAH) and in some cases stroke or death. The size and the location of the aneurysm have been reported as risk factors for hemorrhage (Murayama et al., 1999). When a blood vessel ruptures, bleeding normally occurs in the subarachnoid space but the brain will face severe problems. The tissues may not receive enough oxygen and nutrients. The resulting pressure will cause irritation and swelling. About 20% of strokes happen this way (Brisman, 2009). Some of the symptoms that can be listed include: severe headache, nausea and vomiting, stiff neck, hypertension, loss of balance, blurred vision, photophobia, irritability, and altered level of consciousness (including a deep coma) (Brisman, 2009; University of Virginia Health Center, 2007). Frequent symptoms such as headache, nausea, stiff neck may last for several days.

1.4 Epidemiology

Studies show that the prevalence of cerebral aneurysms in the adult population is between 1% and 5% (Wiebers et al., 2003). It mostly occurs in late 40s and early 60s (A Sadato et al., 1995; Brisman, 2009), and it is more common in women than men (Brisman, 2009). It has also been

estimated that the incidence of SAH from a ruptured aneurysm is approximately 1 case per 10,000 persons in the United States (Schievink, 1997).

1.5 Treatments

There are three main treatments for unruptured cerebral aneurysm: conservative management, surgery, and endovascular treatment (Brisman, 2009). Most clinicians believe ruptured aneurysms should be actively treated, because the risks of a second hemorrhage are so high. The chosen treatment depends on several factors such as: shape, size and location of the aneurysm, age, overall health and medical history, signs and symptoms, presence or absence of risk factors for aneurysm rupture, opinion and preference of the patient. These conditions can also affect the clinical outcome of the treatment (Murayama et al., 1999). There is still no evidence, however, that unruptured aneurysms must be treated.

Surgical treatment, which will be explained in next chapter, is the oldest reported method of treating cerebral aneurysms. However, it is now less in usage because of the emergence of new minimally invasive methods. The most popular endovascular treatment is coil embolization. An important drawback of the endovascular method is the occurrence of recurrences, in 10-30% of cases (Lozier et al., 2002). Therefore, research projects were designed to understand and hopefully minimize this problem. Although the exact mechanism involved in recurrences is unclear, one of the hypotheses is that recanalization originates from the endothelium and that endothelial denudation can prevent recanalization (Jean Raymond et al., 2004). The most recently proposed method to ablate the endothelial lining to prevent recurrences is radiofrequency ablation (RFA) which is still under investigation.

1.6 Objectives

In radiofrequency applications, it is possible to achieve different outcomes by varying energy output, time of application and configuration of the RF electrodes. For RF heating of coils, we wish to ablate the endothelial lining as completely as possible while limiting the risk of damage to surrounding tissues. The main objective of this study will be to investigate the effects of

radiofrequency delivery to the platinum coil (the coil which is placed in the aneurysm in the coil embolization procedure) on temperature and voltage distribution in the surrounding tissues. The reason for monitoring these effects is to optimize the parameters, minimize the risk of recurrences, and minimize the risks of adverse effects. We will consider the effects of following factors on the temperature distribution: coil size, the duration of applied current, the frequency, and the power. The proposed methods to investigate the influence of these specific factors are computer simulation and *in vitro* experiments. The finite element method is used to compute the current distribution in the tissues surrounding a simple coil; the dissipated power density is used to compute the temporal evolution of the temperature distribution. Temperature measurements performed in a similar tissue phantom are used to validate the model.

1.7 Thesis Outline

In Chapter 2, entitled Literature survey and prior results, a brief description of the treatment techniques, their advantages and failures are provided and then, the first attempts at applying RFA are explained. In Chapter 3 the effects of RF in this application is investigated. Chapter 4 will describe the details of the methods used in this study. In Chapter 5 results of the simulations and experiments are shown and discussed. The last chapter will conclude and provide suggestions for future research.

CHAPTER 2. LITERATURE SURVEY AND PRIOR RESULTS

2.1 Introduction

Intracranial aneurysms (cerebral aneurysms or brain aneurysms) relate to a weakening of a brain artery which produces a ballooning of the wall of the artery. As the wall is weakened, it may rupture and lead to stroke or death. We can categorize treatments into two groups: surgical treatments and endovascular treatments (EVT). EVT are minimally invasive, such as coil embolization. In this chapter, the existing treatments, their advantages and drawbacks will be discussed and compared.

2.2 Surgical Treatment

2.2.1 Clipping

The first reported treatment for cerebral aneurysm is surgical clipping which was introduced in 1937 by Walter Dandy, a neurosurgeon at John Hopkins Hospital. Surgical clipping is an invasive method where surgeon will reach the brain by removing part of the skull. A metallic clip will be placed around the neck of the aneurysm, as shown in Figure 2.1, in order to prevent the blood flow from entering the aneurysm. Although surgical clipping is effective, some risk factors are associated with this method. The risk factors associated with this method are the size and location of the aneurysm and the general status of the patient (age, other diseases). According to a study done from 1976 to 1994 in Japan, among 173 patients with subarachnoid hemorrhages (SAH), 115 cases were treated and followed. The cumulative risk for SAH was 1.4% and 12.4% at 10 and 20 years respectively. This study clearly proved the long term efficacy of clipping but also showed that the risk is still present even 20 years after the treatment (Tsutsumi et al., 1999).

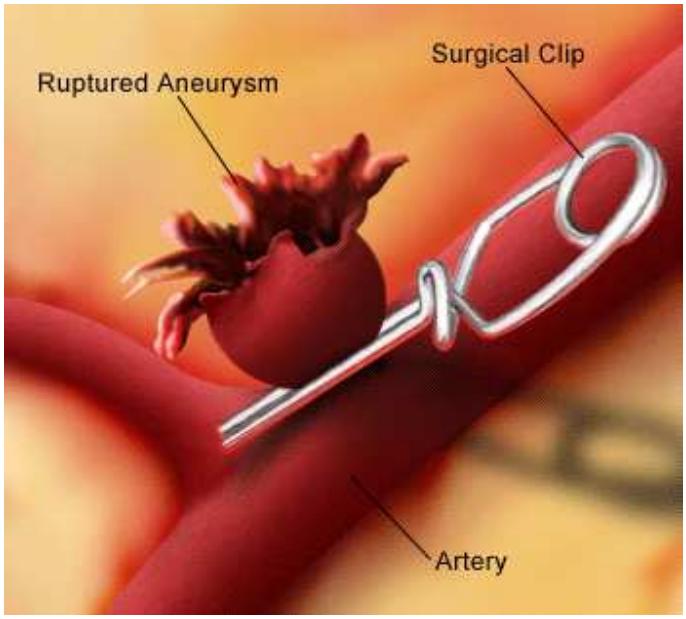

Figure 2.1 Clipping (Yale Medical Group, 2010)

For evaluating the long-term survival of patients who underwent clipping, a retrospective study is reported in 2001. This study was mainly about comparing patients with unruptured aneurysm who did and did not have a clipping. Observed patients were 4619 patients who were hospitalized from 1987 to 2001 because of cerebral aneurysm. The rates of 30-day mortality in patients who underwent surgical clipping with ruptured aneurysm were 13.4% while in the ones with unruptured aneurysm were 5.5%. Follow-up study shows the rates of 17.9% *vs.* 8.5%, 22.4% *vs*. 13.4% and 29% *vs*. 24% at 1, 5 and 10 years respectively (Britz et al., 2004).

Their results showed that among patients with unruptured aneurysm who underwent surgical clipping, the rate of 30-day mortality was 5.5%, while this rate was 7.9% in patients who did not undergo clipping. These rates at 1, 5 and 10 years were 8.5% *vs*. 16.8%, 13.4% *vs*. 30% and 24% *vs*. 44.5%, respectively. Thus, survival estimates for the patients who had the clipping were significantly higher ($P<0.001$) (Britz et al., 2004).

There are multiple methodological flaws in this study however (Jean Raymond et al., 2005).

2.3 Minimally Invasive Treatments

2.3.1 Coiling

Coil embolization or endovascular coiling is the most popular minimally invasive technique to treat cerebral aneurysm. In this method, instead of reaching aneurysm through the skull, a catheter is guided through a blood vessel to reach the aneurysm from an artery in the groin. The catheter is placed inside the aneurysm with the help of fluoroscopic guidance and once it gets there, a thin platinum coil is advanced through the catheter into the aneurysm as shown in Figure 2.2 (Yale Medical Group, 2010).

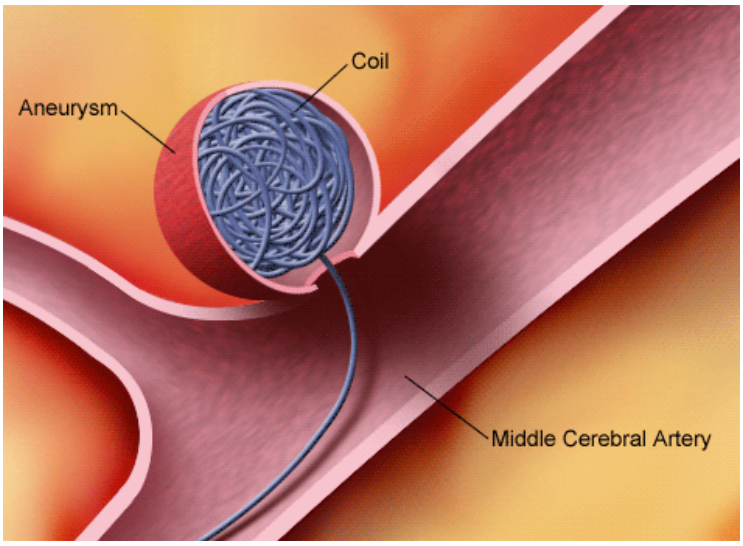

Figure 2.2 Coiling (Yale Medical Group, 2010)

The platinum coil has a helical design with the configuration presented in Figure 2.3. The dimensions of the coil vary according to the application and manufacturers, the typical dimensions of D1, D2, and D3 varies between 44.45 to 76.2 microns, 0.254 to 0.381 mm, and 2 to 20 mm, respectively (White et al., 2008).

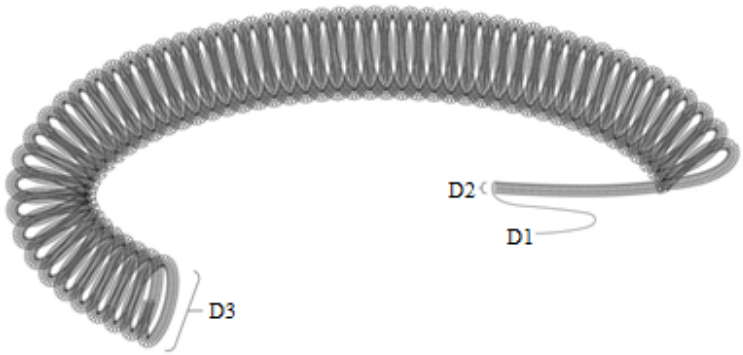

Figure 2.3 Platinum coil configuration (White et al., 2008)

The presence of the coil induces blood clotting, which results in an occlusion in the aneurysm and prevents rupture or re-bleeding. This technique was proposed in 1991 by Guido Guglielmi, a physician at UCLA. The coils are known as Guglielmi Detachable Coils (GDC). They are sometimes used in treatment of some tumors as well. In this application they are utilized to occlude the arteries feeding tumors (Guglielmi, 1998).

The occlusion method is based on two electrochemical principles: electrothrombosis and electrolysis. The cause of electrothrombosis is the negative charges of blood cells and proteins. Positive charges will attract these negative charges and make them form a clot (Guglielmi et al., 1991). The role of electrothrombosis has been clarified by Guglielmi et al. (1991). Their study showed that electrically charged coils will be covered by clot, a phenomenon that is not seen in noncharged coils. They also found that the deposition of blood cells on the coil increases with time (Zucchi et al., 2001). The other phenomenon, electrolysis, happens when a direct electrical current is applied to two immersed iron electrodes. Under these circumstances, the positive end dissolves and the negative one recruits the ferrous ions from the anode to the cathode. Since this phenomenon excludes noble metals, electrolysis will detach the platinum coil from the stainless steel delivery wire (Guglielmi et al., 1991). The detachment procedure will occur after several minutes of application of electrical current. The problem here is that if the number of coils increases, the duration of the procedure will increase as well as the risk of electrothrombosis (A

Sadato et al., 1995). To avoid these risks, another method for detaching the coils was introduced in 1995 by Sadato et al. In this method the coil is detached immediately after applying a monopolar high frequency current. A polyvinyl alcohol (PVA) rod is used at the junction of the coil and the delivery wire. By applying a high frequency electrical current, the heat produced by the current disrupts the PVA junction (A Sadato et al., 1995).

2.3.2 Coiling Method Follow-up Studies

So far, the coiling method has been described. As with any other treatment, some specific problems are associated with this method. The best way to investigate these problems is a follow-up study.

One retrospective study, which started after the introduction of GDC, showed that coil embolization is an effective method for patients suffering from ruptured posterior circulation aneurysms. Before that, treating the posterior circulation aneurysms was more difficult than for the ones located in other areas (Lempert et al., 2000). This study also showed the important role of GDC for patients in poor health condition. The majority of individuals in this study had saccular narrow neck aneurysms and most of the aneurysms were located at the basilar bifurcation. After treatment, recanalization was seen in 22.4% of patients. Most of the recanalization occurred in aneurysms with large neck size or in fusiform aneurysms (Lempert et al., 2000). Another follow-up study done at approximately the same period showed almost the same results and their authors suggested that long-term angiography should be used in order to find additional information (Ng et al., 2002). These studies showed good results for patients who are not good candidates for surgical clipping.

Reported series were thus far uncontrolled and the efficacy and benefit of coiling remained unproved.

Another study was done to investigate the effectiveness of endovascular treatments in conditions where clipping used to be preferred option. In this study, aneurysms located in the middle

cerebral artery (an artery closer to the surface of the surgical field) were treated with the use of GDC. The necks of aneurysms in this area usually are wide and they were considered less favorable for coiling. This study showed that, the mortality and morbidity rate for ruptured aneurysms were 6% and 1% respectively. The mortality and morbidity rate for unruptured aneurysms were 1% and 3% respectively. Recurrences were shown in 20% of patients. Thus, it was concluded that middle cerebral artery aneurysms can also be treated by coiling in most patients and that it is not subjected to neurologic deficits (Iijima et al., 2005).

Recurrences, the recanalization of the aneurysm, are considered more frequent after coiling than after clipping. A study was done amongst all patients treated in a hospital for ten years (Jean Raymond et al., 2003). In this study, recurrences were found in 33.6% of patients after one year. The important factors for the recurrences were listed as: aneurysm size, treatment of ruptured aneurysm, incomplete initial occlusions and duration of follow-up. Standhardt et al. also have done a study to evaluate the results of coiling treatment for unruptured intracranial aneurysms. According to their long term study, the occlusion rate depends on aneurysm size; for increasing aneurysm size, the proportion of completely occluded aneurysms decreased and complete occlusion was observed in 57.5% of cases. The value of this study was that it was done in patients with unruptured aneurysms (Standhardt et al., 2008).

2.3.3 Risks and problems

An important potential complication of EVT is perioperative aneurysmal hemorrhage. According to McDougall et al., the incidence of hemorrhage is low and even if hemorrhage happens, most of the patients will survive without serious problems. The possible factors of iatrogenic rupture may be excessive packing with coils, advancing the guidewire or the coil itself. To avoid rupture, it is important to be aware of the problem, decrease the catheter’s contact time and by not exerting forward pressure on the catheter before removing the guidewire (McDougall et al., 1998).

One of the problems occurring after the treatment is coil compaction. Researches were focused on this matter in 2001, Kawanabe et al. showed the relation between coil packing density and coil compaction (Kawanabe et al., 2001).

One of the other problems associated with the endovascular treatment discussed in follow-up studies, is that the occlusion may not be complete and it may result in recurrences. Some studies have been done to identify risk factors for recurrences. Raymond et al. did a research based on animal models showing that the type of aneurysm is an important factor which determines the degree of occlusion and the ones that are not coiled completely will recur more often (J. Raymond et al., 2008).

2.4 Clipping *vs*. Coiling

So far, the two main methods for treatment of cerebral aneurysms were discussed. Now reviewing the studies in which these treatments are compared might be useful.
International Subarachnoid Aneurysm Trial (ISAT) compared coiling and clipping in a large group of subjects: 2143 patients with ruptured intracranial aneurysms were followed for 6 to 14 years after treatment (Molyneux et al., 2009). The authors concluded that there was an increased risk of recurrent bleeding from coiled aneurysm compared with a clipped aneurysm, but the risks were small and that the risk of death at 5 years was significantly lower in the coiled group than it was in the clipped group. The risk factors for retreatment after 3 months of endovascular treatment are younger age, larger lumen size and incomplete occlusion (Campi et al., 2007).

2.5 Other endovascular treatments

2.5.1 Balloon Occlusion

One of the minimally invasive methods for treatment of cerebral aneurysm is balloon occlusion. This method, which was the first approach to embolization, was introduced by Fedor Serbinenko in 1971 (Linfante & Wakhloo, 2007). This method was helpful in treating the aneurysms that

were inappropriate for clipping because of their size and location (Añon et al., 1992; Ferrito et al., 1994; Meyers et al., 1999).
This method was abandoned after the introduction of GDC coils because it was less effective and more risky in most patients.

2.5.2 Liquid Embolic agents

In the cases where the neck of the aneurysm is too large or irregular, or the location of the aneurysm is not accessible, or performing a surgery can be difficult, parent artery occlusion is the solution, but it is not always possible because of the anatomical location. In such cases, Nishi et al. used an EVAL mixture (Ethylene Vinyl Alcohol Copolymer) as a liquid embolus. They first occluded the parent artery temporarily with a balloon catheter and then injected EVAL through a microcatheter located in the aneurysm (Nishi et al., 1996).
Aburano et al. also used another material when they could not reach the aneurysm. The material was a mixture of NBCA (N-butyl-2-cyanoacrylate) and Lipiodol (iodized oil) (Aburano et al., 2006). Though their aneurysms were on a bronchial artery, the material may be useful for the aneurysms in the brain.

More recently, Vanninen et al. introduced a new liquid embolic material called Onyx for peripheral interventions. It also can be used in combination with coils or balloon catheters. The problem with this material is that it is difficult to control (Vanninen & Manninen, 2007).

Interventions with materials such as balloons and microcoils can be accompanied with rupture or migration of the material to the main vessel, so they are not a good alternative to clipping. However GDC with its adaptability to the shape of aneurysm is a good option (Kawanabe et al., 2001).

2.6 Prior Results

2.6.1 Previous attempts

In order to solve the problems related to coiling, many studies have been done in this area. As it was mentioned earlier, recurrences and recanalization after coil embolization are the most important limitations of this treatment. Now, we will discuss some methods used in order to solve this problem.

Another concept to improve long term results of EVT was used by Murayama et al.: accelerating the “healing process”. They used Bioabsorbable Polymeric Material (BPM), which is a stimulator to inflammation in order to promote neointima formation, in addition to GDC. Although the results of long-term follow-up study are not available, the short-term animal based experiment showed good results (Murayama et al., 2002). Following this study, Taschner et al. did another study with the use of Matrix detachable coils (platinum coils covered with an absorbable copolymer) in order to assess its safety and stability after 6 months. They found that the stiffness of the Matrix coils makes the packing difficult. Their report showed that using the Matrix coils plus bare platinum coils result in stable outcomes (Taschner et al., 2005). Bendszus et al. used a new bioactive coil (Cerecyte) with polyglycolic acid loaded inside of the coil which did not affect the coil. They found that it was safe and potentially more efficient than bare coil, but their study needed to be verified by a prospective randomized trial (Bendszus et al., 2007).

In 2002, Raymond et al. suggested in situ beta radiation to inhibit the cellular process leading to recanalization. Their animal based study demonstrated that low-dose of beta radiation can prevent recanalization and it also showed improvement in short-term result of coil embolization (Jean Raymond et al., 2002). They also performed another study to find out the effects of coil properties and of the location of applied radiation. They concluded that coil properties can minimally affect the recanalization; however the necessary condition for the effectiveness of this process is thrombosis (Jean Raymond et al., 2003). They proved the feasibility of radioactive coils in a human experiment as well, though the long-term result of any damage to the nervous

system is unknown (Taschner et al., 2005). Based on subsequent animal studies, radiation did not show any harmful effects on nervous structure or on neointima formation. However, since clot organization will be influenced by high activities, fixing an upper limit for implanted radioactive is suggested (Jean Raymond, Metcalfe et al., 2006).

One of the hypotheses to be proved to prevent recanalization was endothelial denudation. Raymond et al. performed denudation by the means of an aneurysmal neck-bridge device (ANBD). ANBD is a mechanical device used in order to help placing and retaining the coils into the aneurysm. Though, it is hard to achieve complete denudation and it should be limited to the coiled lesion, endothelial denudation can inhibit recanalization. However, finding a better way rather than ANBD to perform the denudation process would be more convenient, since mechanical denudation is not practical in thin walled or ruptured aneurysms (Jean Raymond et al., 2004). They also suggested cryoablation of the endothelial lining as a substitute method for inhibiting recanalization. They found that cryotherapy can be helpful to some extent in preventing the recanalization, but there exist excessive nerve injuries in their cryotherapy procedure (Jean Raymond, Mounayer et al., 2006). Darsaut et al. assessed stenting combined with endothelial denudation and found that the stent alone cannot produce a solid form to occlude the aneurysm, however their combination will elevate the occlusion and lead to a better result (Tim Darsaut et al., 2007).

2.6.2 *In vivo* Radiofrequency Current Experiments

The latest attempt by Dr Raymond to improve the effectiveness of coil embolization is based on radiofrequency application (Jean Raymond et al., 2010). Radiofrequency current has lots of clinical applications to create targeted lesions, for example, it is widely used for catheter ablation of arrhythmogenic substrates in cardiology. *In vivo* studies were performed in order to show the effects of radiofrequency ablation (RFA) on recanalization. In this application, RFA was likely to denude endothelial layer while having minimum effects on surrounding nervous tissues. Two methods were compared; standard coil embolization and coil embolization followed by RFA of the endothelial lining. The coils (3 to 4 mm 0.015 platinum-tungsten coils 8 to 10 cm in length)

were placed in the arteries. The experiment was done in 6 dogs. In the cases with RFA, a 500 kilohertz (kHz) sinusoidal current with an output power of 20 to 30 W which was adjusted in order to keep the temperature constant at 60°C, was applied to a standard platinum coil for 60 seconds. The tissue surrounding the coil is heated by both resistive heating and conductive heating. Complete occlusion was shown after the procedure in both cases. After two weeks, the results of coil embolization with RF were compared with the results of coil embolization alone, these results suggested that RFA can be effective for both endothelial denudation and improvement of coil embolization, but there is a need to find optimal RFA parameters (power, duration, electrode size, etc.).

2.6.3 *In vitro* Experiments

A first set of *in vitro* experiments was done in order to show the power distribution along the coil. To perform this experiment, a coil (2-5mm caliber 0.015; 2 to 8 cm in length; Boston Scientific) connected to an RF generator (HAT 200, Osypka Company, Germany) was placed in a piece of chicken breast meat. An RF current at 10 watts with a 500 kHz frequency was applied to the coil for 60 seconds. As it is shown in Figure 2.4, the lesion (white) is limited to the first part of the coil. One of the possible causes of this effect may be related to the coil shape; as it was shown previously (Figure 2.3), the coil is rolled up on itself and forms a solenoid whose inductive impedance might oppose the passage of radiofrequency current.

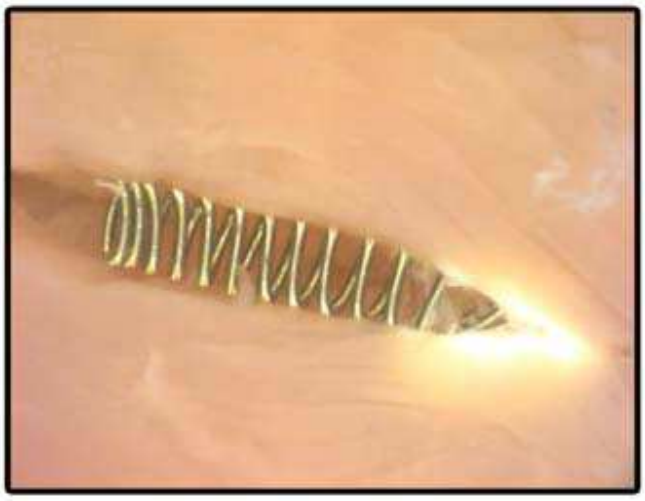

Figure 2.4 Localized lesion after RF transmission through a platinum coil imbedded in a chicken breast (Jean Raymond et al., 2010)

Another experiment was also done by applying a RF current through a stainless steel coil (homemade neurovascular probe) imbedded in an egg white solution. When the temperature reaches a critical value (about 60^{o}C), the solution coagulates (Figure 2.5). The length, caliber and shape of the probe were investigated and it was found that for long probes, the lesion was not be continuous and that short probes had sudden impedance rises and peak temperature. It was found that by increasing the caliber, the lesion area was increased and that the shape of the probe affected the depth of the lesion. The best result is shown in Figure 2.5 where a homogenous lesion was produced.

To investigate the effects of the platinum coil, some preliminary experiments were performed by placing the probe in the middle of a standard platinum coil. This showed the feasibility of the approach and the need for further experiments.

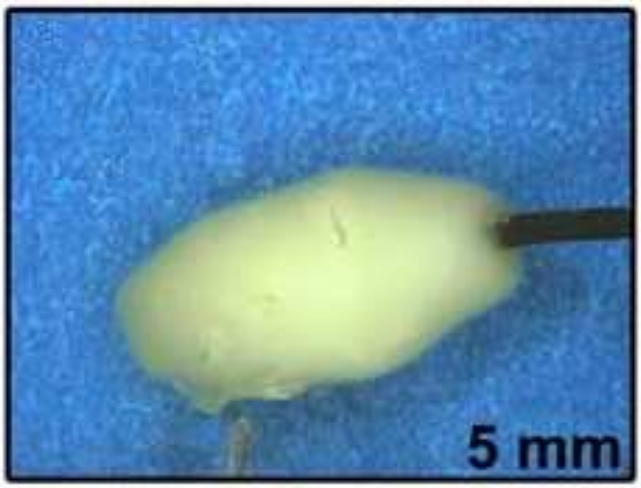

Figure 2.5 Lesion obtained with RF probe (Jean Raymond et al., 2010)

2.7 Summary and Conclusions

This chapter reviewed the studies dealing with the treatment of cerebral aneurysms. Two main treatments were compared and their respective merits were discussed. To improve the coiling technique, radiofrequency ablation was proposed. Based on preliminary *in vitro* and *in vivo* studies which showed the feasibility of this approach, there is a need to further investigate the modalities of radiofrequency current delivery (electrode shape and position, power, duration). In the following chapter, we will thus investigate various parameters that may impact on the efficacy of radiofrequency ablation as applied to this practical problem.

CHAPTER 3. INVESTIGATING THE EFFECTS OF FREQUENCY

3.1 Introduction

We propose to perform both *in vitro* experiments and computer simulations to investigate the parameters and the effects of radiofrequency current applied to an imbedded electrode (platinum coil or applicator) on the temperature distribution of surrounding tissue in order to optimize the RF parameters. For these computer simulations, a very important question that must be answered before constructing a model is whether or not the current distribution depends on the frequency.

At the end of the previous chapter, the preliminary *in vitro* experiments showed that the power distribution along a simple platinum coil is not uniform. A possible explanation for this phenomenon could be that the geometry of the coil creates a large inductive load that blocks the passage of RF current along the length of the coil (Figure 3.1)

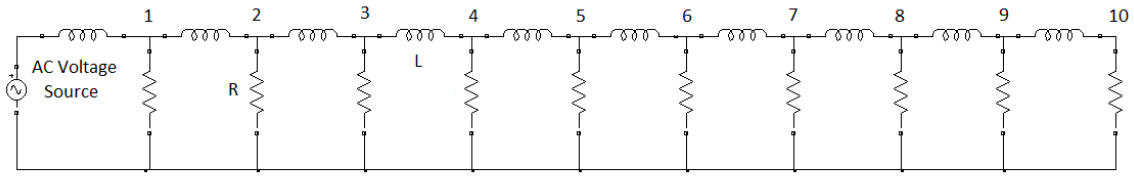

Figure 3.1 Electrical Model of a Coil imbedded in a conductive tissue

According to this hypothesis, the inhomogeneity of the temperature distribution in the tissue surrounding the coil should increase with the frequency of the RF current since the inductive impedance Z_L of a solenoid also increases with the frequency f ($Z_L = j\,2\pi fL$). This increased coil impedance would concentrate the current flow to the tissue near the delivery point of the current to the coil. We will first test this hypothesis by measuring the temperature distribution near a simple coil in a tissue phantom at different frequencies.

3.2 Tissue phantom and experimental setup

The experimental setup consists of a platinum coil (Microplex18 6 mm/15 cm) placed in a cylindrical container (9 cm diameter and 3 mm thickness) filled with a saline gel having the same electrical conductivity as blood (0.67 $S.m^{-1}$). A circular metallic electrode (8 cm diameter) was placed around the coil as a ground electrode to complete the circuit.

An RF current source was applied to the coil. This source consists of a signal generator (Agilent 33220A Function Generator) followed by an RF amplifier (Mini-Circuits ZHL-32A). An oscilloscope (Tektronix TDS3052B) was used to monitor the voltage at two points in order to compute the current and impedance. Three frequencies were investigated: 50 kHz, 500 kHz and 5000 kHz (the frequency used for clinical applications is typically 500 kHz). Figure 3.2 shows the electrical setup.

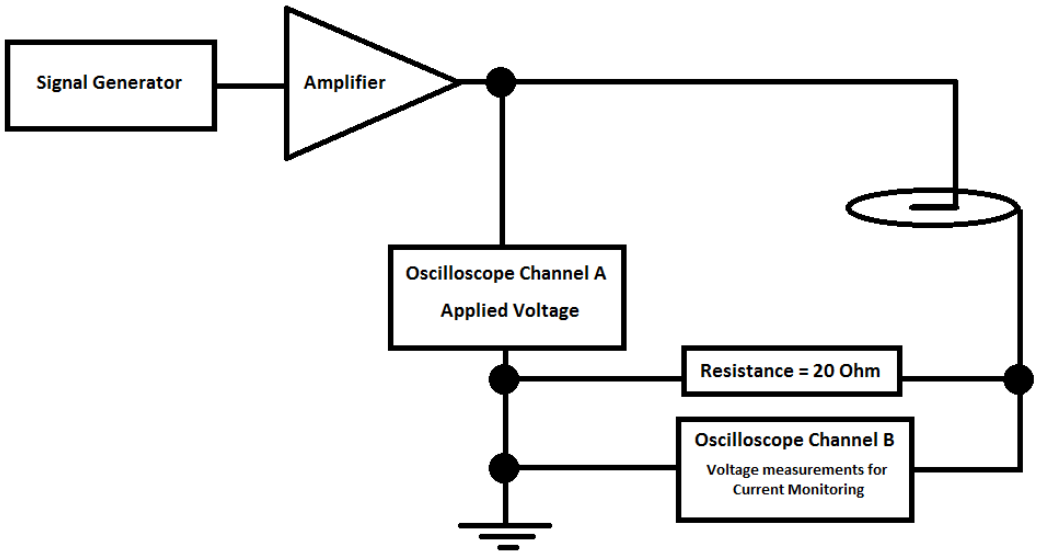

Figure 3.2 Electrical set up

A thin temperature sensitive film, with a color bar showed in Figure 3.3 was placed under the coil and the RF current was applied to one end of the coil. The impedance of the coil as well as the dissipated power were calculated. The gel temperature at two points along the coil (entry point

and the other side) as well near the return electrode (base line) was measured with a thermometer. Photographs of the film were taken to monitor the temperature distribution at different time instants during RF power delivery (2 min, 5 min, and 10 min). The experiment was repeated by applying the RF current to the other end of the coil.

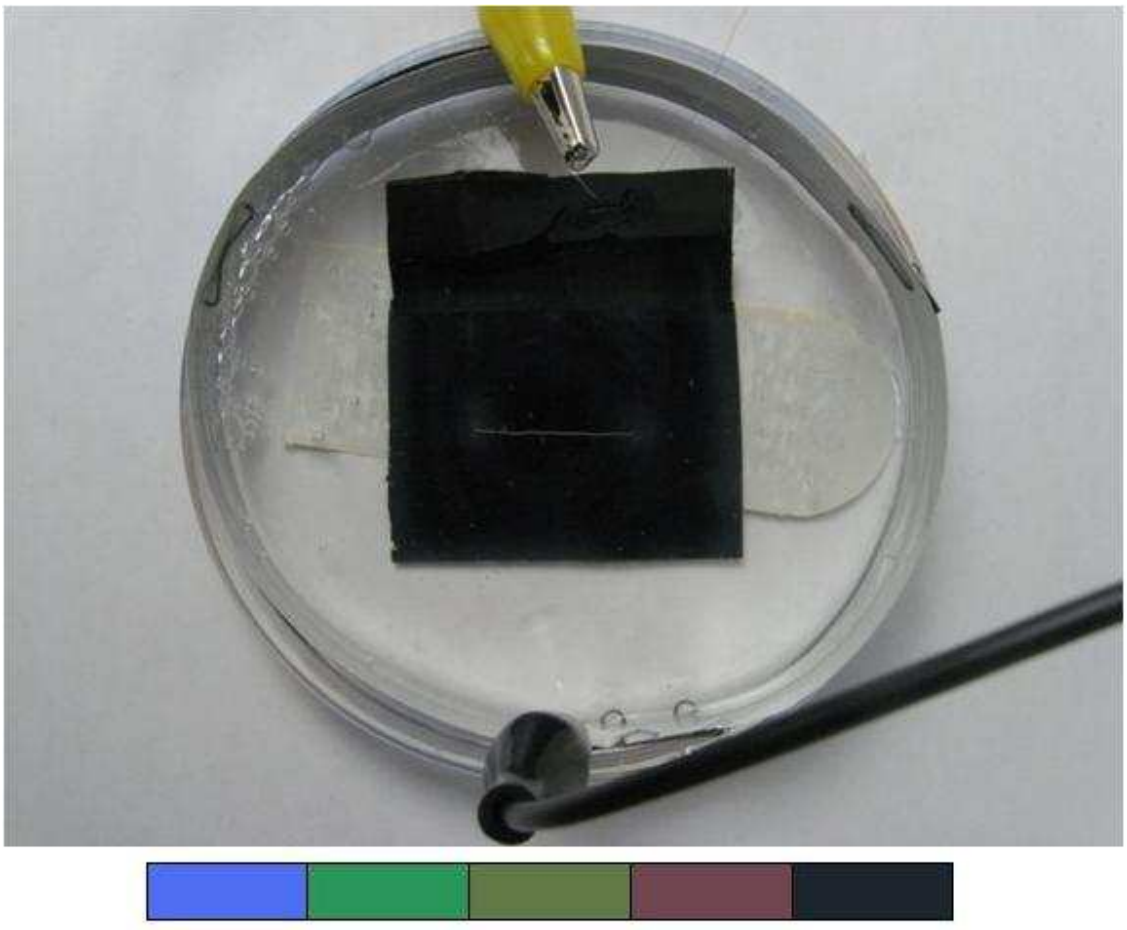

Figure 3.3 A coil immersed in the gel. The color bar shows the different colors of the temperature sensitive film. From left to right, the colors range from highest to lowest temperature with a range of 5 degrees Celsius.

3.3 Effects of frequency on the temperature distributions

The measured parameters are shown in Table 3.1 and the temperature distributions for each applied frequency are shown in the following figures (3.4 to 3.9).

Table 3.1 Electrical and temperature values during RF power application

f(kHz)	A(V)	B(V)	I(A)	P(W)	Z(ohm)	t(min)	T_{base} (°C)	T_{max} (°C)	$T_{otherside}$ (°C)
Applying Radiofrequency Current to the Left side of the coil									
50	23.8	1.54	0.077	1.71	289.1	2	20.8	25	23
50	23.8	1.54	0.077	1.71	289.1	5	20.8	26	23.5
50	23.8	1.54	0.077	1.71	**289.1**	10	20.8	26.6	24.1
500	25.8	1.65	0.0825	1.99	292.7	2	20.8	25.9	23.5
500	25.8	1.69	0.0845	2.04	285.3	5	20.8	27.9	24.9
500	25.8	1.7	0.085	2.05	**283.5**	10	20.8	28.8	25.3
5000	24.8	1.54	0.077	1.79	302.1	2	20.8	25.9	23.3
5000	24.8	1.54	0.077	1.79	302.1	5	20.8	26.8	24.3
5000	24.6	1.56	0.078	1.80	**295.4**	10	20.8	27.3	24.9
Applying Radiofrequency current to the Right side of the coil									
50	24	1.47	0.0735	1.66	306.5	2	20.8	24.9	23.4
50	24.1	1.49	0.0745	1.68	303.5	5	20.8	26.1	24.3
50	23.8	1.51	0.0755	1.68	**295.2**	10	20.8	26.8	25.1
500	24.2	1.51	0.0755	1.71	300.5	2	20.8	25.4	23.6
500	24.2	1.51	0.0755	1.71	300.5	5	20.8	26.3	24.8
500	24.2	1.51	0.0755	1.71	**300.5**	10	20.8	27.1	25.1
5000	25.2	1.5	0.075	1.78	316.0	2	20.8	25.5	24.2
5000	25.2	1.51	0.0755	1.79	313.8	5	20.8	27,4	25.2
5000	25.2	1.51	0.0755	1.79	**313.8**	10	20.8	27.5	25.4

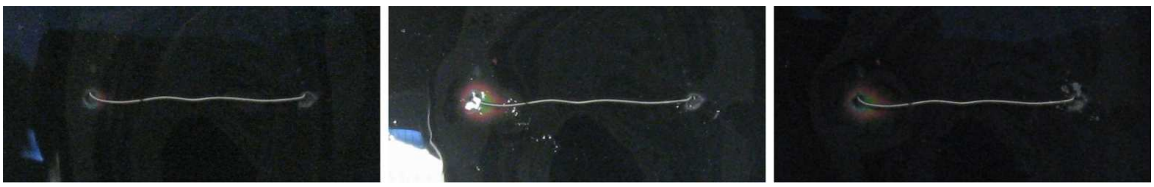

Figure 3.4 Temperature distribution after 2 minutes with RF applied to the left side of the coil, from left to right: f = 50 kHz, 500 kHz, 5000 kHz

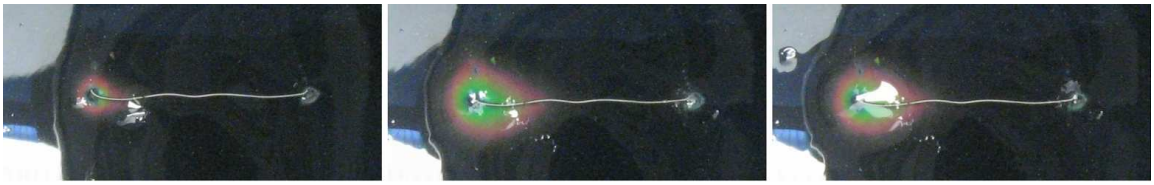

Figure 3.5 Temperature distribution after 5 minutes with RF applied to the left side of the coil, from left to right: f = 50 kHz, 500 kHz, 5000 kHz

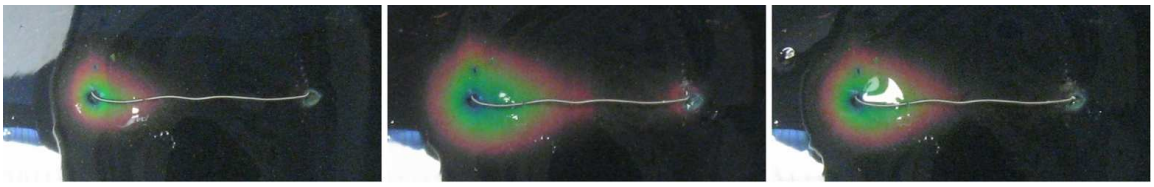

Figure 3.6 Temperature distribution after 10 minutes with RF applied to the left side of the coil, from left to right: f=50kHz, 500kHz, 5000kHz

Figure 3.7 Temperature distribution after 2 minutes with RF applied to the right side of the coil, from left to right: f=50kHz, 500kHz, 5000kHz

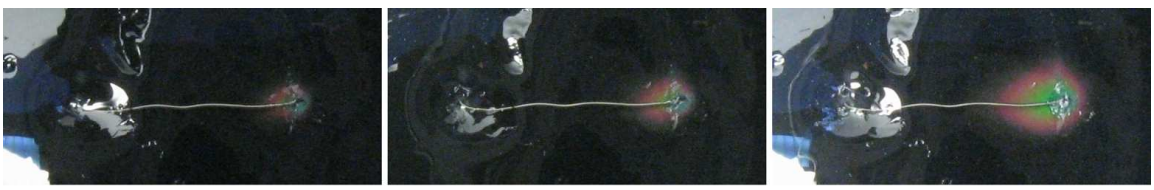

Figure 3.8 Temperature distribution after 5 minutes with RF applied to the right side of the coil, from left to right: f = 50 kHz, 500 kHz, 5000 kHz

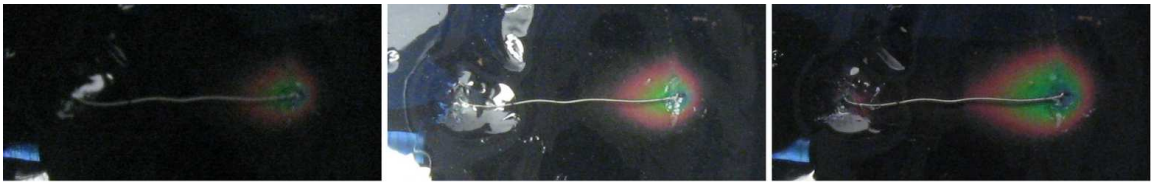

Figure 3.9 Temperature distribution after 10 minutes with RF applied to the right side of the coil, from left to right: f = 50 kHz, 500 kHz, 5000 kHz

By observing the highlighted impedance values in Table 3.1, it can be found that there are no significant changes in impedance for the three frequencies. The dissipated power also remains at about 1.8 W, whatever the frequency, the current delivery site or the time instant. The maximum temperature at one time instant is also not affected by the frequency.

Similarly, as can be seen in the figures, the power is always dissipated near the current delivery site whatever the frequency or the delivery site. The temperature is always much higher around the delivery site and the lack of uniformity of the temperature distributions along the length of the coil is not modified by changing the frequency.

Therefore, the non uniformity of the temperature distributions cannot be explained by the inductive impedance of the coil and the exact mechanism for the non-uniform distributions remains unclear and there is a need to perform some other experiments to understand this phenomenon.

3.4 Investigating the impedance of a simple coil

The input impedance of a circuit may comprise a resistive as well as a reactive component (inductive for a coil). If the temperature inhomogeneity cannot be attributed to inductive effects as shown in the previous section, it could be attributed to a resistive effects. To investigate this second hypothesis, the amplitude of the impedance *Z*, its phase and the resistance *R* of different coils were measured at different frequencies (Table 3.2).

Table 3.2 Impedance and Resistance of different kind of coils at different frequencies

Name of the Company & Ref#	Length (cm)	f (kHz)	Z (ohm)	Phase (degree)	Impedance in 1 cm (ohm)	R (ohm)	R in 1Cm (ohm)
Boston Scientific	30	50	131.1	0	4.37	179.9	5.997
Ref 352163-4		500	128.5	3	4.28		
		5000	139.1	12	4.64		
Boston Scientific	6	50	275.9	1	45.99	199.8	33.3
Ref 350620-3		500	276.9	2	46.15		
		5000	258.2	3	43.03		
Boston Scientific	30	50	597.3	0	19.91	440	14.667
Ref 350730-3		500	589.9	0	19.66		
		5000	530.0	2	17.67		
Boston Scientific	11.5	50	563.3	1	48.99	475	41.304
Ref 342515-4		500	565.1	2	49.14		
l size=15		5000	517.0	8	44.96		
HELIPAQ microcoil	10	50	733.7	0	73.37	545	54.5
Ref HSR100410-20		500	735.0	2	73.5		
		5000	651.6	7	65.16		
Axium	8	50	629.4	0	78.67	376	47
Ref QC-4-8-HELIX		500	631.2	2	78.9		
		5000	544.9	11	68.12		
HyperSoft Helical	6	50	925.5	0	154.24	645	107.5
Ref 100306HS-V		500	923.5	2	153.92		
		5000	778.2	10	129.71		
Unknown	5	50	259.2	0	51.84	175	35
Ref 340308-4		500	264.8	2	52.97		
		5000	238.4	3	47.68		

The results show that for all the coils under investigation, their impedance *Z* remains almost constant whatever the frequency. However, the resistances *R* of all coils tend toward the value of impedance *Z*. This outcome supports the second hypothesis: that power is dissipated mostly at the current delivery site because of a resistive effect of the coil.

As shown in Figure 2.3, the coil is a very thin long platinum wire, rolled up on itself. Since the resistance *R* of a wire is inversely proportional to its cross section, the high resistance of the coil

can be explained by its very small cross section since the resistance is proportional to the inverse of the cross section area:

Equation 3.1 $$R = \rho \frac{L}{A}$$

where R is the resistance (Ω), ρ is the resistivity (Ω-m), L is the length (m) and A is the cross section area (m^2).

3.5 Conclusion

We conclude from the results presented in this chapter that we can neglect the effects of frequency for the modeling of the coil and of the tissue, and that both can be considered to behave as purely resistive media for the frequencies that are typically used in the clinic (500 kHz).

CHAPTER 4. ELECTROTHERMAL MODELING

4.1 Introduction

For the computer simulations, the finite element method was used to compute both the current distribution and the temporal evolution of the temperature distribution in the tissue. The objective was to optimize the radiofrequency parameters in order to create a homogenous and predictable temperature distribution.

4.2 Theoretical analysis

The COMSOL® Multiphysics 3.5a (a finite element analysis and solver software for engineering applications) was employed to produce different finite element models. Before computing the temperature distributions, first we have to find the power density produced by the current. The model should satisfy the following equation for electrical analysis:

Equation 4.1 $$\nabla.(\sigma \nabla V) = 0$$

where σ (S m^{-1}) is the electrical conductivity of the tissue (that depends on tissue type and temperature) and V (V) is the potential. The boundary conditions required to solve the preceding equation are a constant electrical potential over the active electrode surface (a constant voltage is applied to one end of the electrode), a nul potential on the surface of the return electrode, and nul current density over the interfaces between the conductive medium and surrounding dielectric media. The power density P_d (W m^{-3}) dissipated by the current flow in the tissue can be calculated by:

Equation 4.2 $$P_d = \sigma(\nabla V)^2$$

The temperature is governed by the bio-heat equation which is a parabolic partial differential equation. It was first proposed by Pennes to describe heat transportation in living tissue. The equation is defined as:

Equation 4.3 $$\rho C \, {}^{\partial T}/_{\partial t} + \nabla.(-k\nabla T) = \rho_b C_b \omega_b (T_b - T) + Q_{met} + Q_{ext}$$

Where ρ (kg m^{-3}) is the tissue density, C (J kg^{-1} °C^{-1}) is the specific heat of the tissue, T (°C) is the local temperature at any given time, t (s) is time, k (W m^{-1} °C^{-1}) is the thermal conductivity of the tissue, ρ_b (kg m^{-3}) is the density of blood, C_b (J kg^{-1} °C^{-1}) is the specific heat of blood, ω_b (kg m^{-3} s^{-1}) is the blood perfusion rate, T_b(°C) is the arterial blood temperature, Q_{met},(W m^{-3}) is a metabolic heat source and Q_{ext} (W m^{-3}) is the spatial heat source.

4.3 High resistance coil model

The first coil model which was used to obtain our preliminary results consists of a thin cylindrical shape with a length of 2 centimeters, immersed in another cylindrical shape having similar geometrical, thermal and electrical properties as the phantom described in the preceding chapter. The model is shown in Figure 4.1 and the values of all constants and parameters for this model are given in Table 4.1.

Once the model is created, the software constructs the mesh (Figure 4.2) and performs the potential and temperature computations. Images of the temperature distribution, voltage distribution and temperature changes by time are shown in the next chapter.

Table 4.1 Parameters and constants of the platinum coil model

	σ	ρ	C	k	ρ_b	C_b	ω_b	T_b	Q_{met}	Q_{ext}
Unit	S m^{-1}	kg m^{-3}	J kg^{-1} °C^{-1}	W m^{-1} °C^{-1}	kg m^{-3}	J kg^{-1} °C^{-1}	kg m^{-3} s^{-1}	°C	W m^{-3}	W m^{-3}
milieu	0.67	4200	1000	0.63	0	0	0	22	0	P_d
coil	167	2800	1000	73	0	0	0	22	0	0

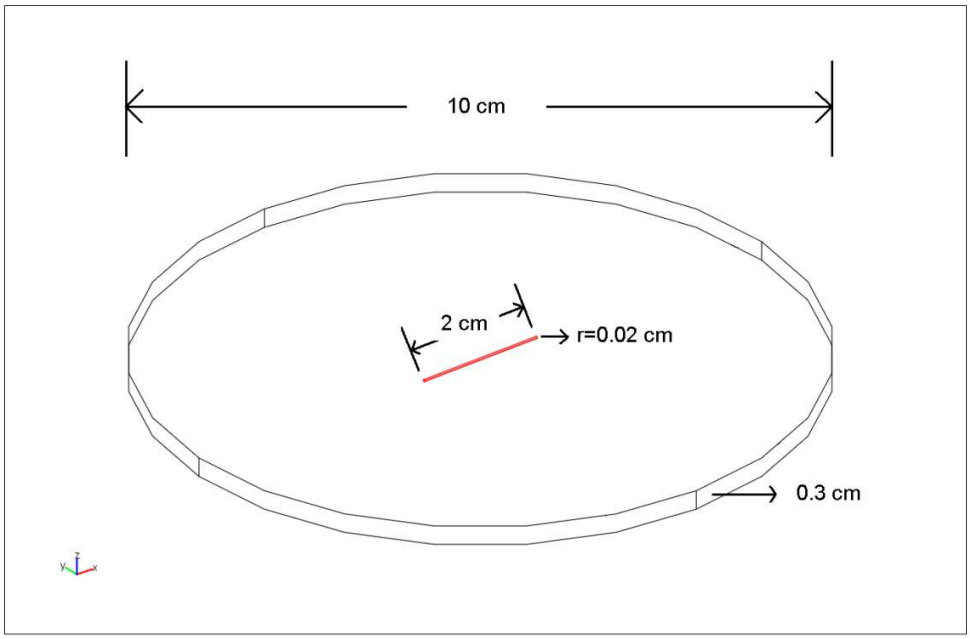

Figure 4.1 Geometry of the first model

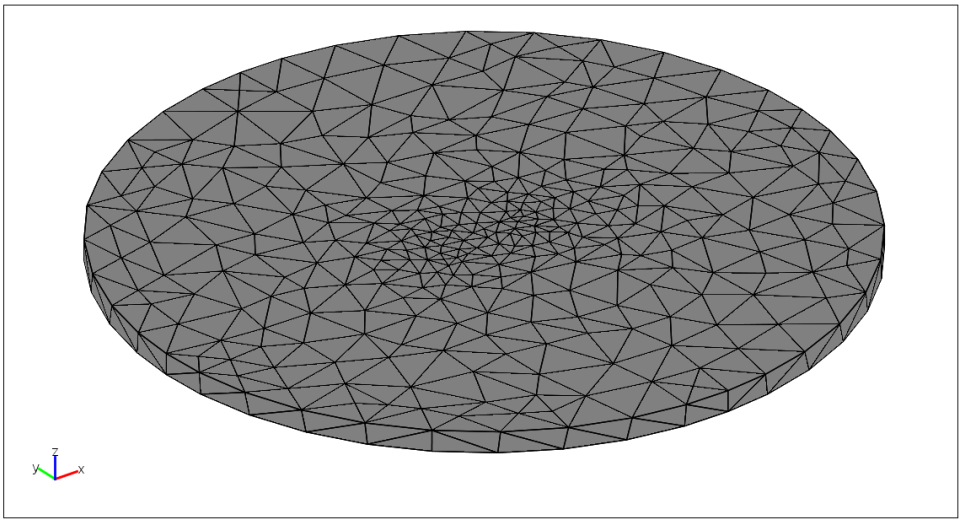

Figure 4.2 Mesh created by COMSOL

The values provided in Table 4.1 are mostly obtained from (Kaouk et al., 1996). The equivalent electrical conductivity for the electrode was calculated from our measurements of the resistance

of a typical coil so as to simulate the high resistance coils that were described in the preceding chapter. The heat from metabolic activities is neglected as well as the heat transfer by the blood flow. The external heating is the resistive heating (P_d) produced by the radiofrequency current (equation 4.2).

4.4 Low resistance applicator model

Based on the results obtained from the *in vitro* experiments that showed nonuniform temperature distributions because of the high resistance of the coil, it was suggested to apply the current not to a coil, but to a low resistance applicator. We thus created a model consisting of a solid stainless steel electrode, instead of a platinum coil, with the same volume conductor geometry as the previous model using the following parameters and values (Table 4.2); i.e. platinum characteristics substituted by steel characteristics.

Table 4.2 Parameters and constants of the stainless steel applicator model

	σ	ρ	C	k	ρ_b	C_b	ω_b	T_b	Q_{met}	Q_{ext}
Unit	S m^{-1}	kg m^{-3}	J kg^{-1} °C^{-1}	W m^{-1} °C^{-1}	kg m^{-3}	J kg^{-1} °C^{-1}	kg m^{-3} s^{-1}	°C	W m^{-3}	W m^{-3}
milieu	0.67	4200	1000	0.63	0	0	0	22	0	P_d
coil	4.03e6	7850	475	44.5	0	0	0	22	0	0

As it was found that the potential distribution along the steel applicator is almost uniform, it was needed to optimize the size of the applicator to have a uniform temperature distribution as well. Thus the steel applicator model was modified to investigate the effects of different lengths and cross section radius of the applicator to investigate the influence of electrode size on the temperature distribution and to find its optimum size. Stainless steel applicators with cross section radii equal to 100 µm, 150 µm, and 200 µm with different lengths of 3 mm, 6 mm, 10 mm, 15 mm and 20mm were studied. The observed parameters were the voltage distribution, temperature distribution and temperature changes versus time, which are presented in the next chapter. To compare the results with those of the high resistance coil, models of a platinum coil with a cross section radius equal to 200 µm and different lengths were also made.

4.5 Applicator-in-coil model

In the previous models of stainless steel applicators, a helical platinum shape was also added in order to investigate the influence of platinum coil. The steel applicator was placed in the middle of a platinum coil shown in Figure 4.3. The voltage was applied to one end of the applicator and not to the coil directly. The temperature distribution, voltage distribution and temperature changing versus time of all the models which consists of different size of steel applicator are shown in the next chapter.

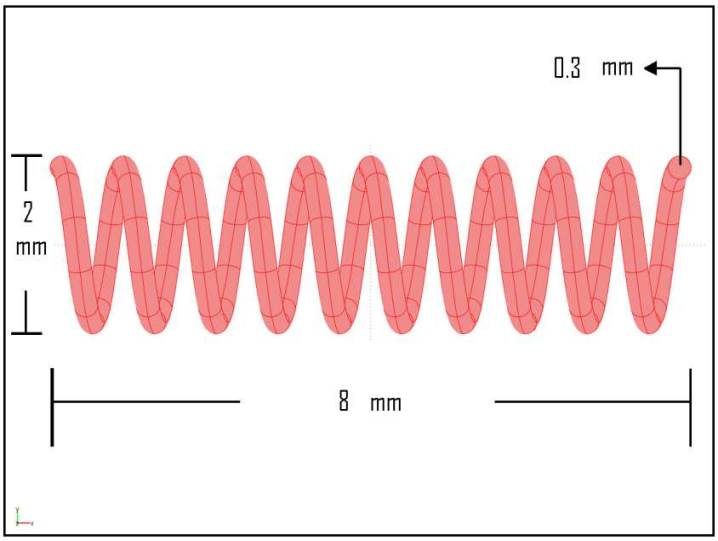

Figure 4.3 Model of a platinum coil which will be placed around the steel applicator

4.6 Effects of Mesh Size on the Simulation Results

In solving partial differential equation problems, using a larger number of elements will lead to a more accurate result. In the problems with small dimensions (in the order of 0.1 mm), similar to our application, solving the models with more elements will imply longer computation time and may not be necessary. Thus, we performed simulations for some selected models with different numbers of elements to study the convergence of our simulations. The mesh was thus refined four times, the number of elements was increased and the results were monitored. In the next

chapter the number of elements and the differences are presented. The comparison is done with the low resistance steel applicator alone and the applicator-in-coil model.

4.7 Additional simulations and experiments

After finding the optimal size of the applicator to produce a uniform temperature distribution, there was a need to validate the results with an *in vitro* experiment. Thus, an applicator with a diameter of 0.46 mm was placed in the experimental set up described in the previous chapter and the temperature distribution was monitored while applying an RF current with the frequency of 500 kHz to different length of the applicator (3 mm, 6 mm, 10mm, 15 mm, and 20 mm). Different parameters (voltage, current, power, and maximum temperature) were observed at different times (2, 5, and 10 minutes) which their values are all gathered in a table in the next chapter.

Since in the previous computer models, the caliber of the applicator does not match the one in the experimental study, after completing this experiment, models with the same size and characteristics were also created in COMSOL® to compare the results with the experimental one and to validate the simulation results.

4.8 Applicator-in-coil experiments and modeling

The preceding section was related to the study of the temperature distribution around different sizes of applicators in the absence of platinum coil in order to optimize the size of the applicator. In real applications, there will be a platinum coil in the aneurysm, thus there is a need to investigate the effects of the presence of the high resistance platinum coil. The same experiment as described in section 4.7 was repeated while placing the applicator in the middle of a platinum coil with the following characteristics; length 8 mm, radius 2m m, cross section radius 0.19 mm. The same set up was used and as in the other experiments, the length of the steel applicator was changed to observe the changes for each length. Voltage, current, power and temperature at different times (2, 5 and 10 minutes) were monitored. The results of this study are shown in the next chapter.

As in the previous simulations, the steel applicator with different sizes, as mentioned above, was simulated in the middle of a solenoid platinum coil (Figure 4.4) and the same parameters (voltage and temperature distribution) were observed. The results will be compared and discussed in the next chapter.

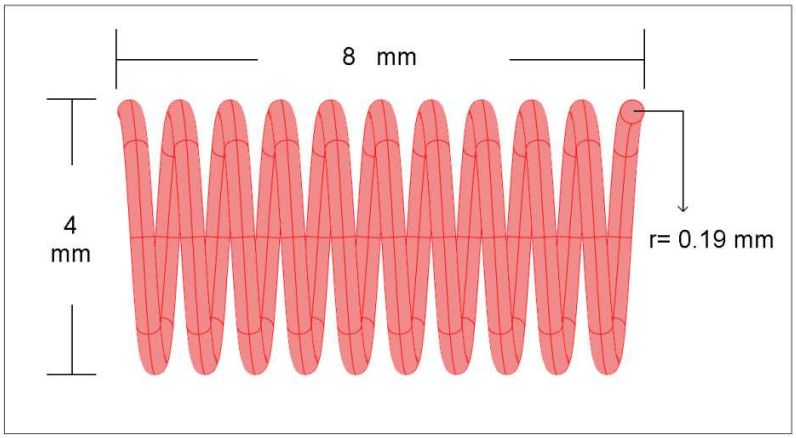

Figure 4.4 Model of a solenoidal platinum coil

4.9 Applicator-in-brain model

Computer simulations were also done in a model with similar characteristics as the brain. The model consists of a large cylinder (with a diameter and height equal to 8 cm) representing the brain tissue and a small cylinder in the middle of the big one acting as a steel applicator as it is shown in Figure 4.5. The simulation was done with two optimized lengths of coils (6 mm and 10 mm) with a diameter of 0.46 mm to find the optimal voltage and duration of application.

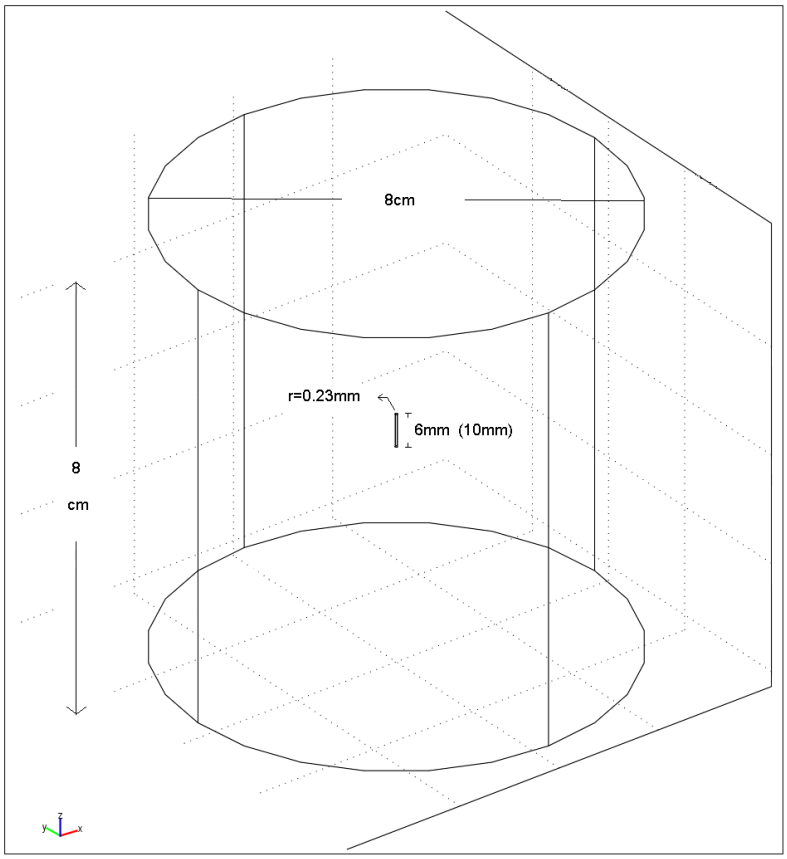

Figure 4.5 Applicator-in-Brain Model

The voltage with different values (5, 10, 15V) was applied to one end of the coil and the temperature distribution, voltage distribution, and temperature rise in the first 120 seconds of application were monitored. The parameters of this model are presented in Table 4.3. The results are shown in the next chapter.

Table 4.3 Parameters and constants of the Brain Model

	σ	ρ	C	k	ρ_b	C_b	ω_b	T_b	Q_{met}	Q_{ext}
Unit	S m^{-1}	kg m^{-3}	J kg^{-1} °C^{-1}	W m^{-1} °C^{-1}	kg m^{-3}	J kg^{-1} °C^{-1}	kg m^{-3} s^{-1}	°C	W m^{-3}	W m^{-3}
milieu	0.15	1050	3700	0.5	0	0	0	37	0	P_d
coil	4.03e6	7850	475	44.5	0	0	0	37	0	0

4.10 Temperature dependant electrical conductivity

A final simulation was done in the brain model using variable electrical conductivity. The value of the electrical conductivity, as well as depending on the type of the tissue, weakly depends on the temperature and it can be calculated by this equation:

Equation 4.4 $$\sigma = 1/(\rho_0(1 + \alpha(T - T_0)))$$

Where σ (S m^{-1}) is the electrical conductivity, ρ_0 (Ω m) is the resistivity at reference temperature, α (°C^{-1}) is the temperature coefficient, T (°C) is the temperature and T_0 (°C) is the reference temperature.

In our application, the tissue temperature changes and it can affect the electrical conductivity. Thus, a simulation was made in order to show the effects of a variable electrical conductivity and to determine whether or the electrical conductivity can be considered constant. For each temperature rise of 1°C, the electrical conductivity rises by 2% because of electrolytic effects (Shimko et al., 2000). The values of the parameters are presented in table 4.4. The results of the simulation are shown and discussed in the next chapter.

Table 4.4 Parameters of Equation 4.4

	ρ_0	α	T_0
Unit	Ω m	°C^{-1}	°C
milieu	6.67	-0.02	37

CHAPTER 5. MODELING AND EXPERIMENTAL RESULTS

5.1 Introduction

In this chapter, the results obtained with the models described in the previous chapter are presented, discussed and compared.

5.2 High Resistance Coil Simulations

The first model was that of a 2 cm long and a 0.02 cm cross section radius electrode with an equivalent conductivity similar to that of an endovascular coil placed in a cylindrical shape. Figure 5.1 shows the voltage distribution and Figure 5.2 shows the steady state temperature distribution around the coil while applying 17.86 V to one end of the coil. The maximum temperature which is occurred at the current entry point was 31.5°C. In Figure 5.3, the temperature against time at different points is plotted.

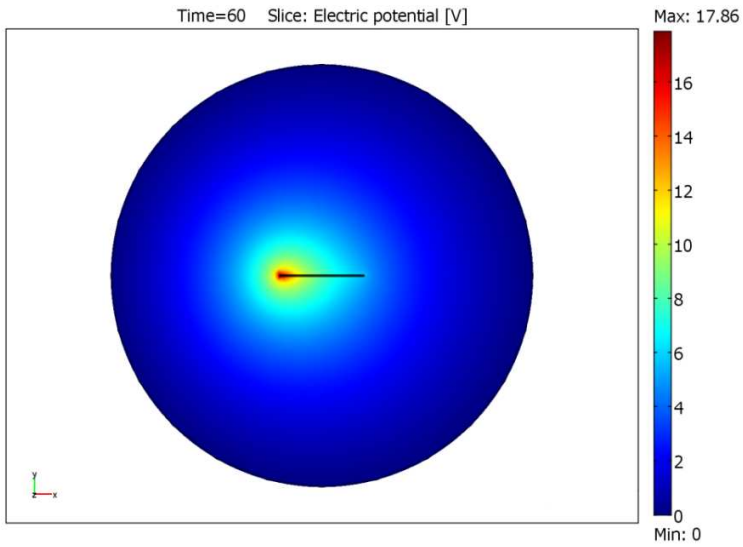

Figure 5.1 Voltage distribution in the high resistance coil model.

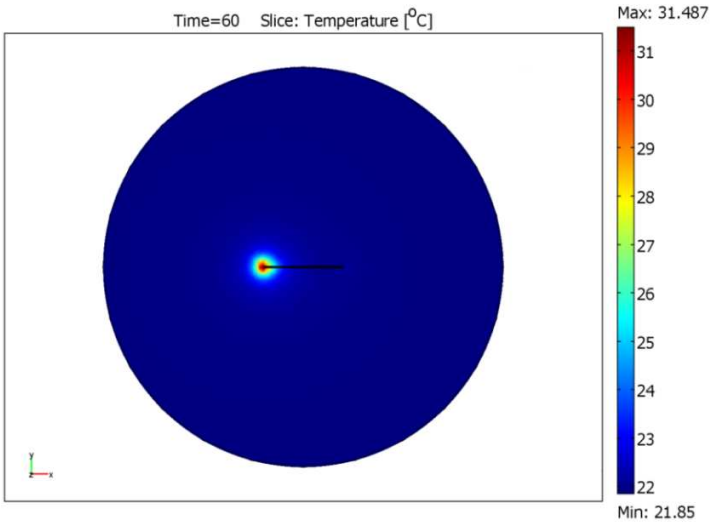

Figure 5.2 Steady state temperature distribution for the high resistance coil model.

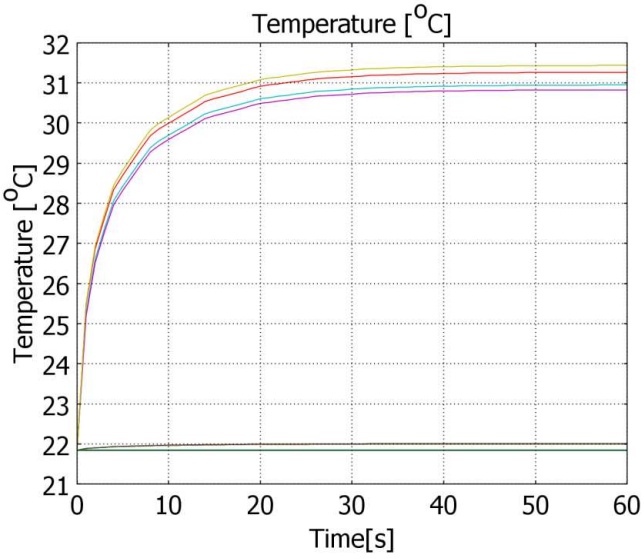

Figure 5.3 Temperature *vs* time at different points in the high resistance coil model. The upper 4 curves (yellow, red, blue, purple) illustrate the temperature at 4 points in the vicinity of the current entry point. The 2 lowest curves (black, green) correspond to parts of the other end of the coil (black) and the periphery (green).

As can be seen in these figures, the voltage and the temperature are not distributed uniformly along the length of the coil, they are highest at the beginning of the coil. This non uniform temperature distribution along the length of the coil corresponds to what was observed in our previous *in vitro* studies. The decrease of potential along the coil confirms our second hypothesis that the non uniform temperature distribution is due to the high resistance of the coil relative to the surrounding media.

5.3 Low Resistance Applicator Simulations

In order to have a more uniform temperature distribution, it was suggested to apply the radiofrequency current to a low resistance applicator instead of applying it directly to the endovascular coil. Thus, to find the effects of the coil's resistance on the temperature distribution, the same model with the same dimensions but with the conductivity of solid stainless steel was made. The same voltage was applied to the end of the applicator. The voltage and temperature distributions are shown in Figures 5.4 and 5.5 respectively. The voltage is now completely uniform along the length of the applicator because of its low resistance (Figure 5.4), while the temperature is now identical at both ends of the applicator (Figure 5.5). The temperature is highest at both ends of the applicator because of the higher current density due to the higher potential gradient at both ends. Figure 5.6 demonstrates the temperature changes at different points against time, and it can be seen that a steady state is reached after about 20 seconds.

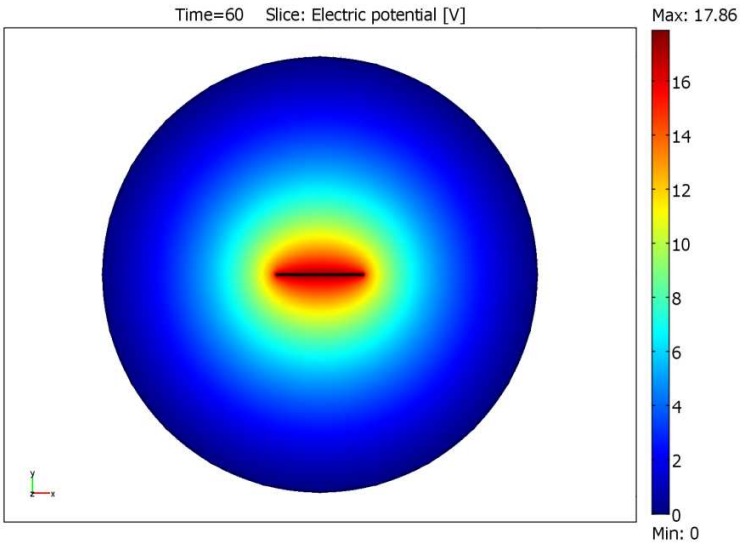

Figure 5.4 Voltage distribution for the low resistance applicator model.

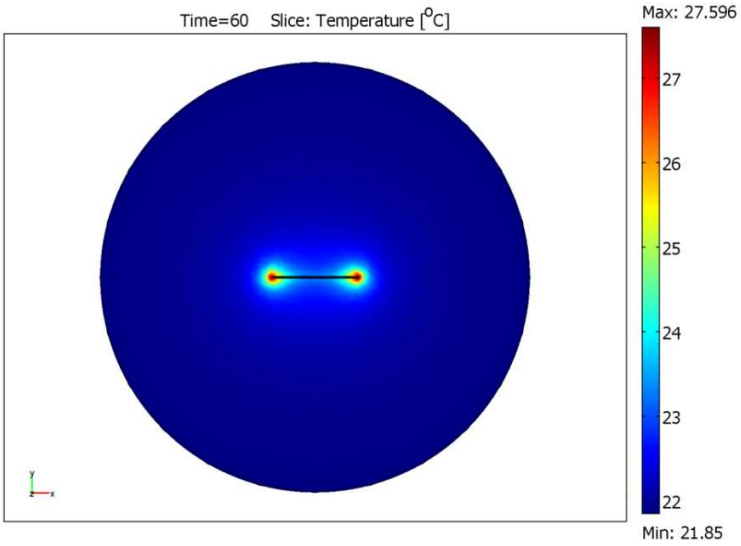

Figure 5.5 Steady state temperature distribution for the low resistance applicator model.

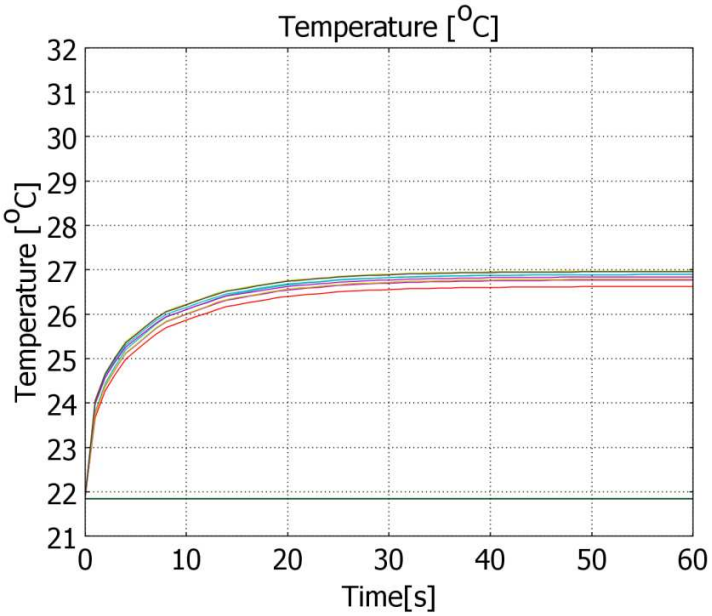

Figure 5.6 Temperature *vs*. time at different points in the low resistance applicator model. The upper curves illustrate the temperature at the vicinity of both ends of the applicator. The lowest curves correspond to the periphery.

5.4 Applicator and Coil Size Optimization

In Figure 5.5, it can be seen that the temperature increase is focused at both ends of the applicator. Can we change the size of the applicator in order to have a more uniform temperature distribution along the whole length of the coil? The low resistance applicator model was thus modified to investigate different sizes of the applicator (radius equals to 100 µm, 150 µm, 200 µm and length equals to 3 mm, 6 mm, 10 mm, 15 mm and 20 mm). The voltage distributions are not shown here since the applicator was always equipotential as in Figure 5.4 because of its low resistance. However, the dimensions of the applicator had a significant effect on the uniformity of the steady state temperature distributions which are shown in Figure 5.7 to 5.11. The effects of the applicator's length and radius on the maximum temperature are also summarized in Table 5.1.

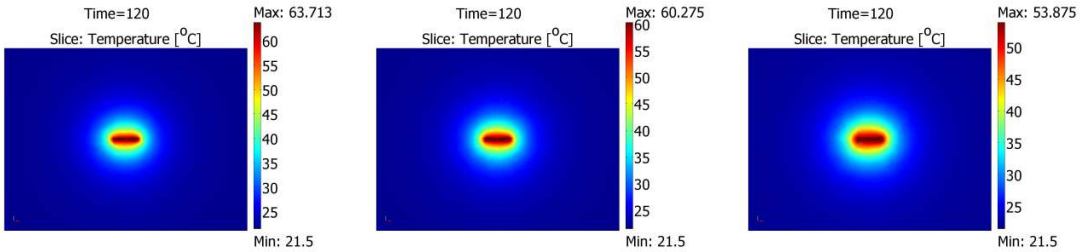

Figure 5.7 L = 3mm, from left to right r = 100 µm, 150 µm, 200 µm.

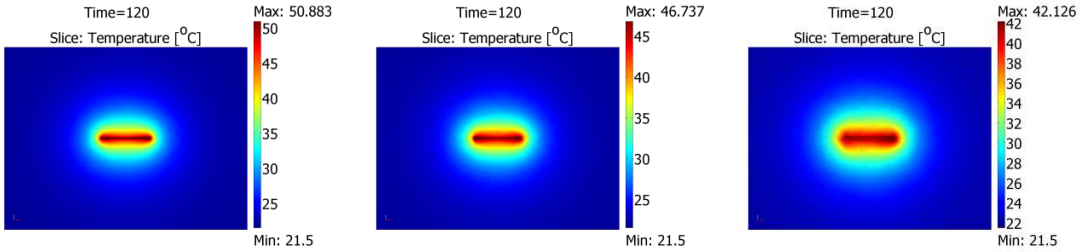

Figure 5.8 L = 6 mm, from left to right r = 100 µm, 150 µm, 200 µm.

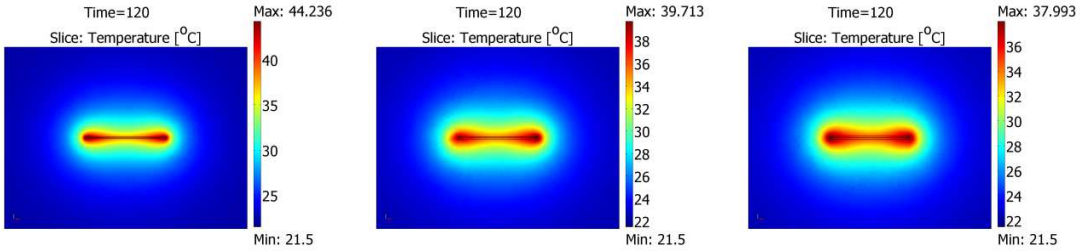

Figure 5.9 L = 10 mm, from left to right r = 100 µm, 150 µm, 200 µm.

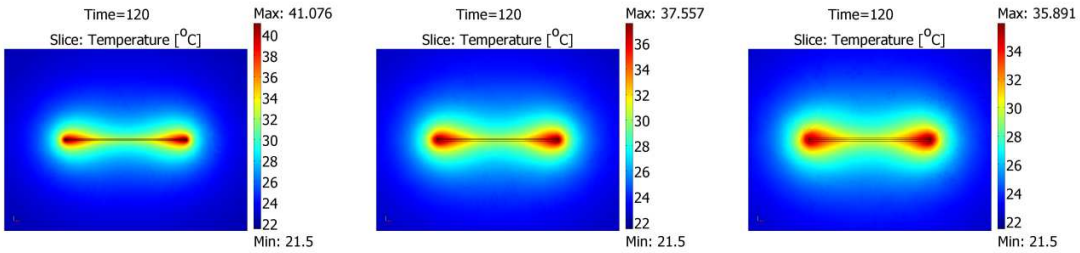

Figure 5.10 L = 15 mm, from left to right r = 100 µm, 150 µm, 200 µm.

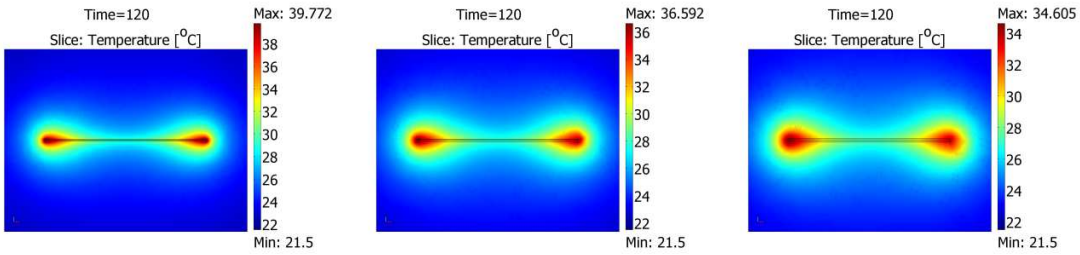

Figure 5.11 L = 20 mm, from left to right r = 100 µm, 150 µm, 200 µm.

Table 5.1 Effects of the dimensions of the applicator on the maximum temperature.

	r = 0.001 mm					r = 0.0015 mm					r = 0.002 mm				
	L (mm)					L(mm)					L(mm)				
	3	6	10	15	20	3	6	10	15	20	3	6	10	15	20
Max T (°C)	63.7	50.9	44.2	41.1	39.8	60.3	46.7	39.7	37.6	36.6	53.9	42.1	38.0	35.9	34.6

Observing Figures 5.7 to 5.11, it can be found that the maximum temperature is always highest at both ends of the applicator, but that the shorter applicators tend to have temperature distributions with circular and symmetrical patterns that are more uniform. The longer electrodes have two distinct temperature extreme at both ends with a “Q-tip” like pattern. Applicators with a smaller radius tend to have the highest temperature at both ends, but with a larger temperature gradient (Table 5.1). To produce a uniform temperature distribution, applicators having a radius of 200 µm and a length between 6 mm and 10 mm would be satisfactory.

The following figures show the results for the high resistance coil model with a radius of 200 µm and different lengths (3 mm 10 mm and 20 mm). This was done to assess the differences between low resistance applicators and high resistance coils for all lengths. As it can be seen in all of these pictures, none of them is demonstrating a uniform temperature distribution.

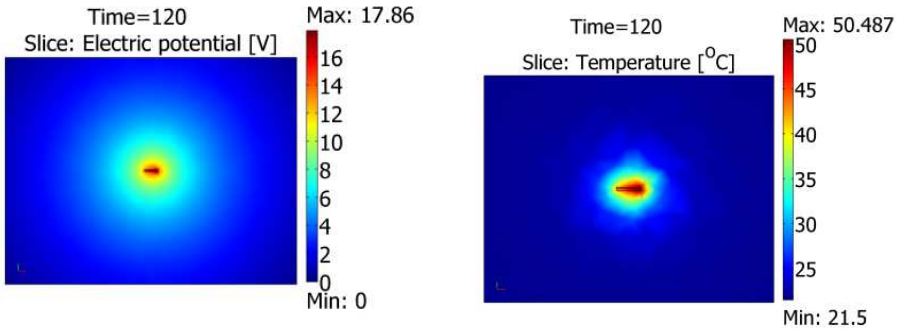

Figure 5.12 L = 3 mm, From left to right, voltage and steady state temperature distributions for the high resistance coil model.

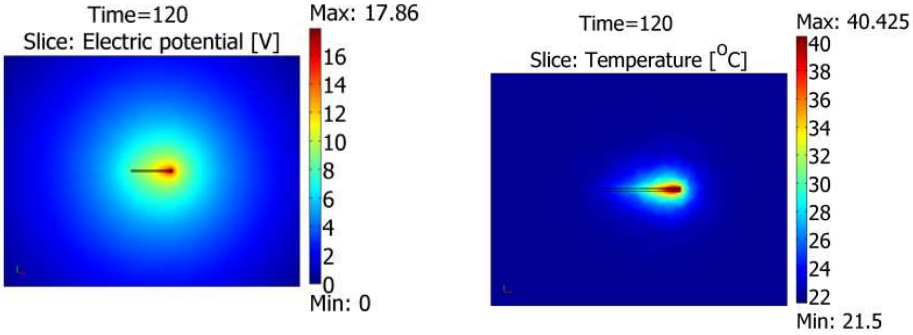

Figure 5.13 L=10 mm, From left to right, voltage and steady state temperature distributions for the high resistance coil model.

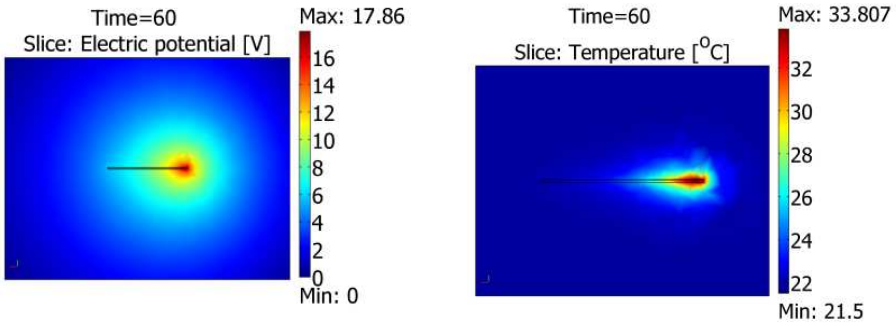

Figure 5.14 L= 20 mm, From left to right, voltage and steady state temperature distributions for the high resistance coil model.

5.5 Applicator-in-Coil Simulations

The influence of a platinum coil around the steel applicator is not clear. Thus, in order to assess its influence, the same low resistance applicator with different sizes is placed in the middle of a platinum coil as described in previous chapter. The steady state temperature distributions for these models are shown in following figures and Table 5.2 summarizes the maximum temperature for different sizes of the low resistance applicator when it is placed in the middle of a high resistance platinum coil.

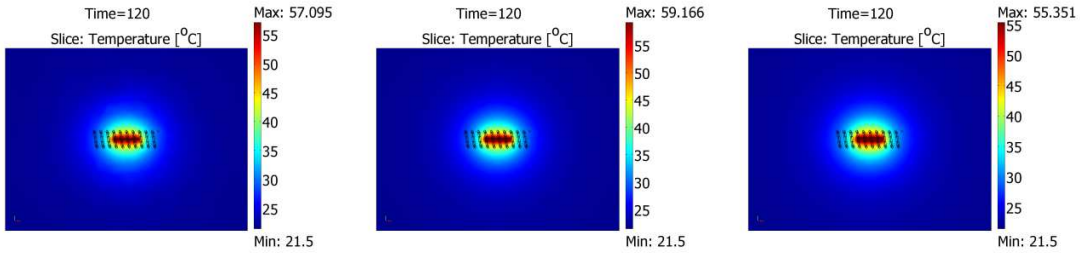

Figure 5.15 L = 3 mm, from left to right r = 100 µm, 150 µm, 200 µm.

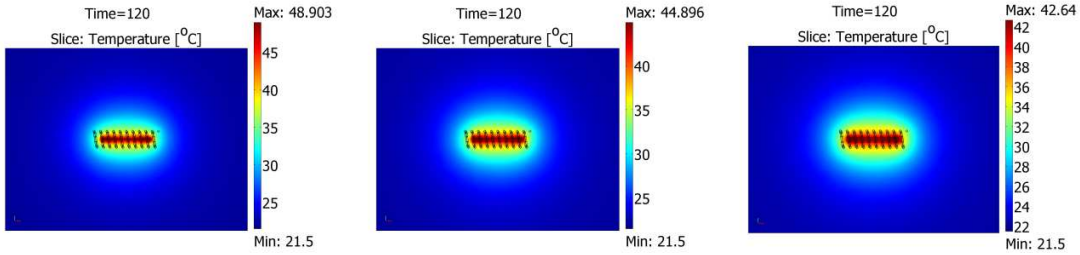

Figure 5.16 L = 6 mm, from left to right r = 100 µm, 150 µm, 200 µm.

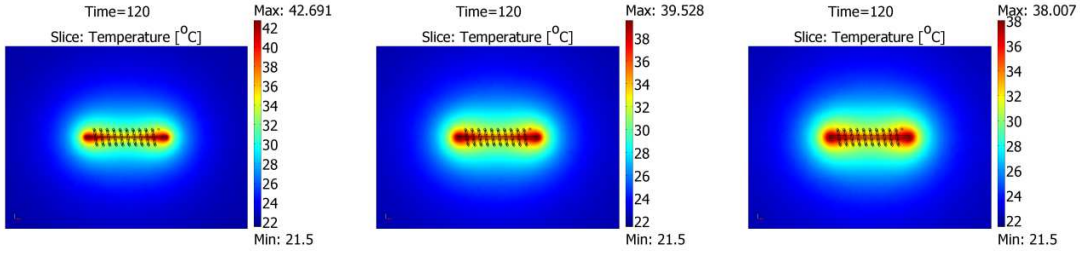

Figure 5.17 L = 10 mm, from left to right r = 100 µm, 150 µm, 200 µm.

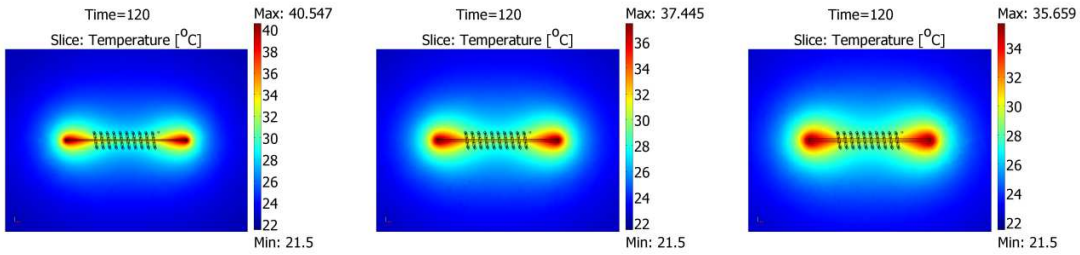

Figure 5.18 L = 15 mm, from left to right r = 100 µm, 150 µm, 200 µm.

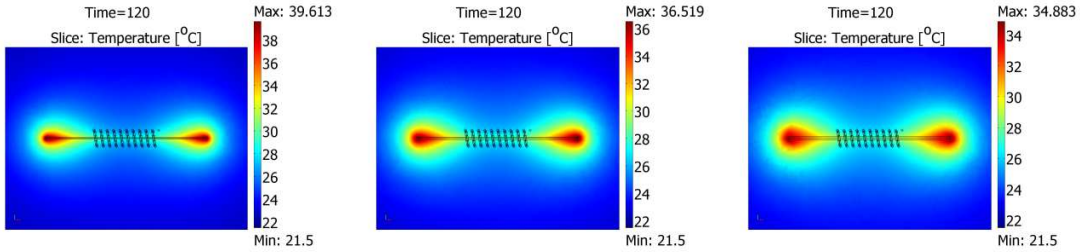

Figure 5.19 L = 20 mm, from left to right r = 100 µm, 150 µm, 200 µm.

Table 5.2 Effects of the dimensions of the applicator in a coil on the maximum temperature.

	r = 0.001 mm					r = 0.0015 mm					r= 0.002 mm				
	L (mm)					L (mm)					L (mm)				
	3	6	10	15	20	3	6	10	15	20	3	6	10	15	20
Max T (°C)	57.1	48.9	42.7	40.5	39.6	59.2	44.9	39.5	37.4	36.5	55.35	42.6	38.0	35.7	34.9

The effects of placing a high resistance platinum coil around a low resistance applicator are minimal for the steady state temperature distributions, but it produces slightly more uniform temperature distributions for the longer applicators (lessening of the “Q-tip” effect). This could be attributed to the thermal conductivity of the coil which is higher than that of the tissue. The coil thus tends to be isothermal. In Table 5.2, there is only a slight decrease in the maximum temperature in the models with a smaller radius, when the platinum coil is placed around the stainless steel applicator.

5.6 Effects of Mesh Size

As it was said in solving a partial differential equation problem, a larger number of elements will lead to a more accurate result. Since solving all the created models with finer mesh would take a long time, we checked the accuracy of our results in a few models. Simulations were performed with different mesh size in order to validate our results. The mesh was refined four times and the results were compared. A comparison was made in two groups of models; the low resistance applicator and the applicator-in-a-coil. This comparison was done in models with different sizes of steel applicator and the results are presented in Table 5.3.

Table 5.3 Effects of mesh size on maximum temperature

			low resistance applicator		applicator-in-coil	
Series #	Radius (μm)	Length (mm)	Number of Elements	Temperature °C	Number of Elements	Temperature °C
1	100	3	2002	63.713	19862	57.095
			7627	67.307	78839	60.434
			26253	69.148	265421	62.73
			87475	69.381	881294	64.426
2	100	6	3071	50.883	19695	48.903
			12572	52.063	78298	49.548
			43423	52.843	263523	49.804
			146410	52.886	872641	49.8
3	100	10	4409	44.236	21320	42.691
			18534	44.73	84964	43.247
			63918	45.144	285322	43.587
			214772	45.205	941582	43.528
4	100	15	6027	41.076	22898	40.547
			26235	41.49	91370	41.013
			89353	41.881	306709	41.332
			300513	41.828	1013521	41.238
5	100	20	7106	39.772	23586	39.613
			30930	40.267	95011	39.955
			105738	40.672	320086	40.326
			355347	40.719	1059687	40.366
6	150	3	1709	60.275	19336	59.166
			6595	62.564	77487	59.92
			22577	63.405	261467	60.16
			74917	63.486	867467	59.773

7	150	6	1995	46.737	19453	44.896
			7569	48.003	77499	45.216
			25344	48.587	260673	45.438
			84243	48.619	863071	45.406
8	150	10	2465	39.713	20402	39.528
			9522	41.053	81856	40.12
			32591	41.747	275857	40.274
			108435	41.749	912862	40.274
9	150	15	3230	37.557	21069	37.445
			13147	38.303	84809	37.949
			45112	38.773	284748	38.327
			152306	38.879	940457	38.287
10	150	20	3731	36.592	21365	36.519
			15266	37.287	86860	37.156
			52790	37.766	293142	37.594
			180092	37.841	973157	37.623
11	200	3	1448	53.875	19452	55.351
			5126	56.511	78148	55.669
			16612	58.166	263432	55.642
			53468	58.639	872457	55.292
12	200	6	1637	42.126	19677	42.64
			5941	44.373	78754	42.928
			20072	45.465	265936	42.847
			65492	45.793	880320	42.629
13	200	10	2106	37.993	20221	38.007
			8100	38.95	80632	38.231
			26870	39.566	270884	38.254
			88741	39.53	894944	
14	200	15	2551	35.891	20566	35.659
			10004	36.509	82768	36.129
			33729	36.862	278752	36.374
			112953	36.826	919943	
15	200	20	2883	34.605	20609	34.883
			11477	35.319	83476	35.466
			39095	35.984	281467	35.791
			131467	35.94	931394	

Figures 5.20 and 5.21 show the curves of maximum temperature obtained using the four mesh sizes for the two models: low resistance applicator and applicator-in-coil. For the last three mesh refinements of the applicator-in-coil model, we could not get the results because the computation time was too long (in the order of days).

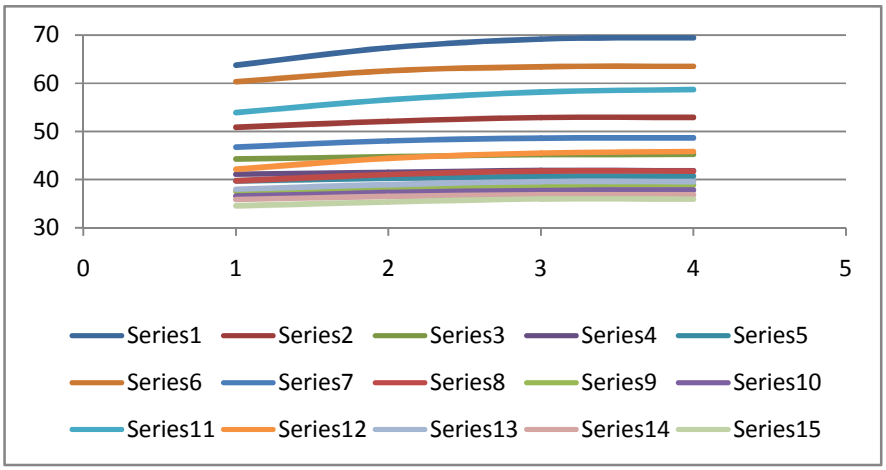

Figure 5.20 Maximum temperatures for the four mesh sizes in the applicator model.

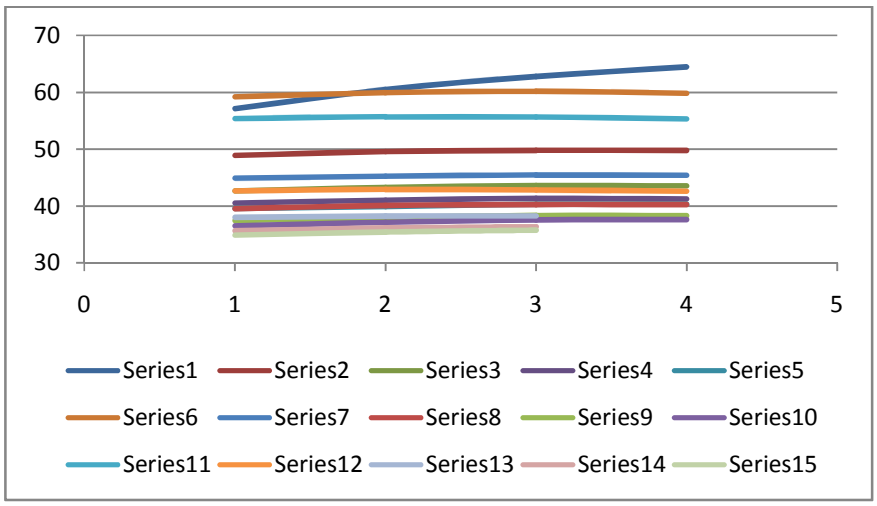

Figure 5.21 Maximum temperatures for the four mesh sizes in the applicator-in-coil model.

As it is presented in previous table and pictures the temperature change can be neglected in all models –except in the first two models- as it is less than 1 degree Celsius. In the first two models the change is more significant, but still cannot be a concern of this study because it was found that the size of those models are so small and it is not appropriate for the application. Thus, the resolution used in this study is equal to the lower one and there is no need to have more elements to be significantly more precise.

5.7 Additional Applicator Experiments and Simulations

Our proposed method is to inject the radiofrequency current in a low resistance applicator placed in the middle of a platinum coil. Previous simulations show that this method can produce more uniform temperature distributions. Additional *in vitro* experiments were done in order to validate these simulations. A steel applicator with a 0.23 mm radius was placed in the same experimental set up as described in Chapter 3 and a RF voltage source with a 500 kHz frequency was connected to the applicator. This experiment was repeated for different lengths of applicator (3 mm, 6 mm, 10 mm, 15 mm, and 20 mm), in order to optimize the parameters. The electrical and temperatures measurements for different lengths are shown in Table 5.4, and the temperature distributions obtained with the temperature sensitive film are shown in following figures.

Table 5.4 Electrical and temperatures measurements for different lengths of applicator

Length (mm)	A (V)	B (V)	I (A)	P (W)	Z (ohm)	t (min)	Tbase °C	Tmax °C
3	15.7	0.961	0.04805	0.71	306.7	2	22.5	25.8
3	15.4	1.04	0.052	0.75	276.2	5	22.5	26.7
3	15.6	0.982	0.0491	0.72	297.7	10	22.5	27.3
6	14.7	1.28	0.064	0.86	209.7	2	22.5	24.6
6	14.4	1.34	0.067	0.88	194.9	5	22.5	26.5
6	14.5	1.32	0.066	0.87	199.7	10	22.5	27.1
10	14.7	1.28	0.064	0.86	209.7	2	22.5	24.2
10	14.1	1.34	0.067	0.85	190.4	5	22.5	25.1
10	14.7	1.22	0.061	0.82	221.0	10	22.5	26.7
15	13.7	1.6	0.08	0.97	151.3	2	22.5	24.1
15	13.5	1.66	0.083	0.98	142.7	5	22.5	25.1
15	13.6	1.56	0.078	0.94	154.4	10	22.5	26.5
20	13.5	1.66	0.083	0.98	142.7	2	22.5	24
20	13.3	1.72	0.086	1.00	134.7	5	22.5	25
20	13.3	1.71	0.0855	0.99	135.6	10	22.5	26.3

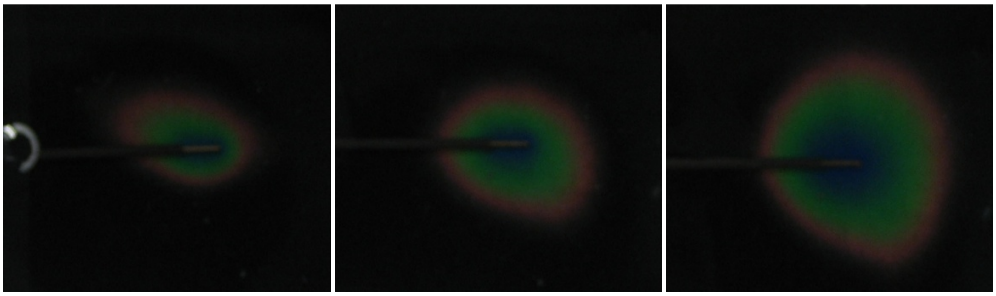

Figure 5.22 L = 3 mm, images taken after 2, 5, 10 minutes.

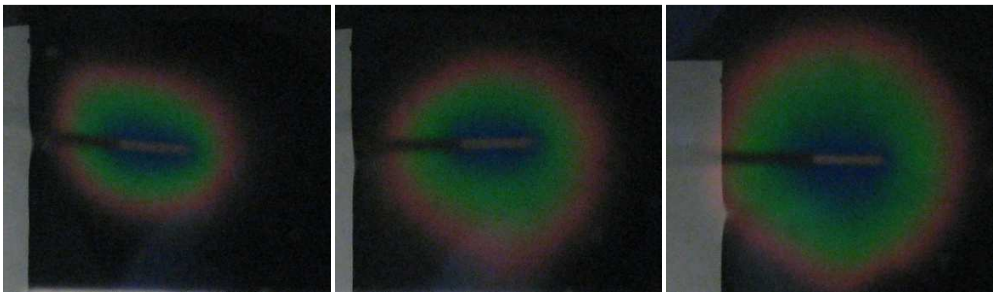

Figure 5.23 L = 6 mm, images taken after 2, 5, 10 minutes.

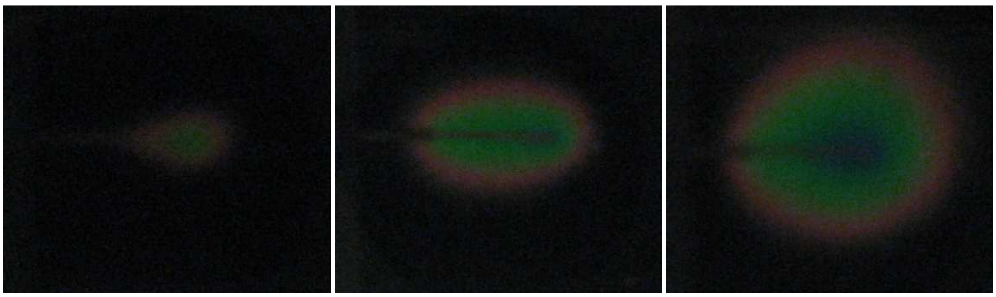

Figure 5.24 L = 10 mm, images taken after 2, 5, 10 minutes.

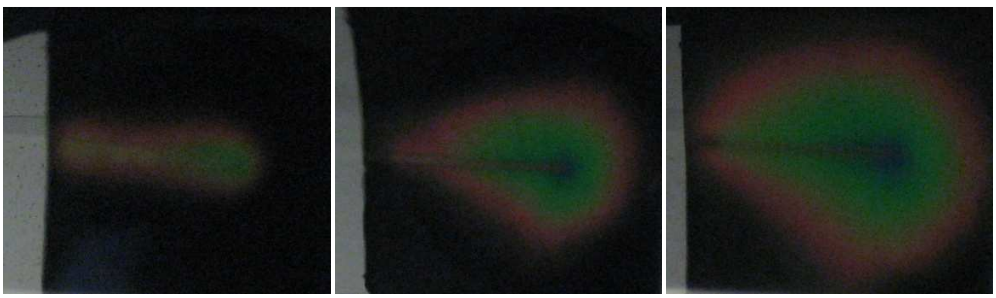

Figure 5.25 L = 15 mm, images taken after 2, 5, 10 minutes.

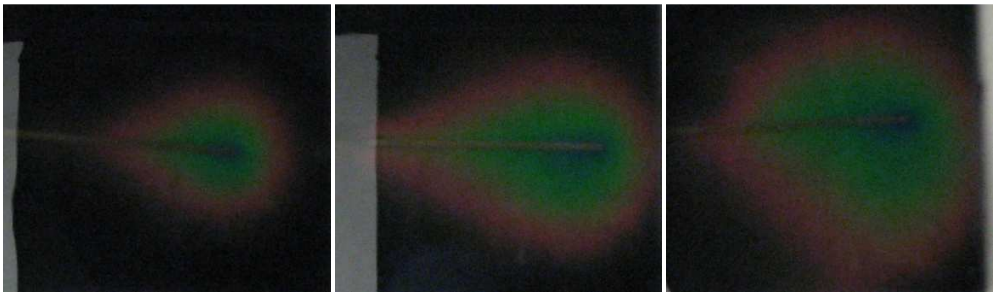

Figure 5.26 L = 20 mm, images taken after 2, 5, 10 minutes.

The following figures are the results of computer simulations. Models with the same size and characteristics as the *in vitro* experiment were created. In each picture, from left to right, the voltage distribution, temperature distribution and temperature versus time are illustrated.

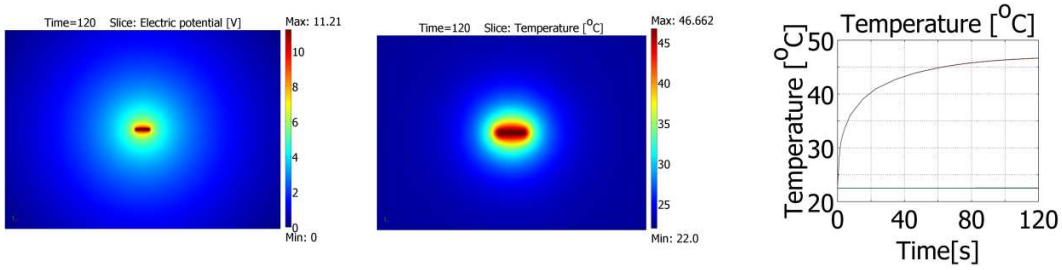

Figure 5.27 Applicator simulation results, L = 3 mm.

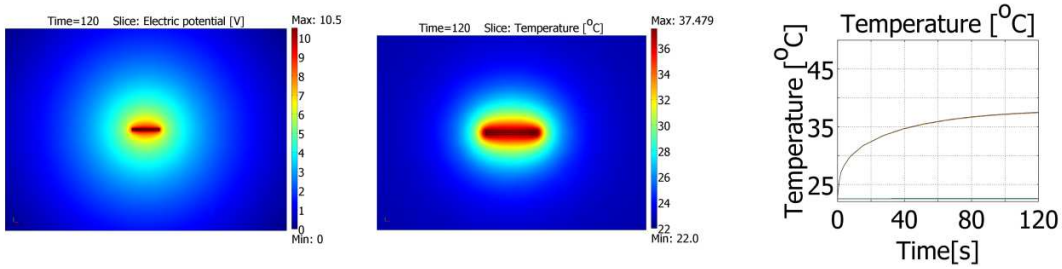

Figure 5.28 Applicator simulation results, L= 6 mm.

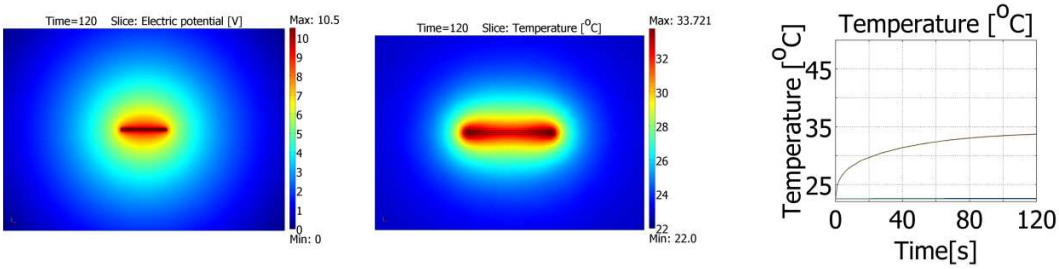

Figure 5.29 Applicator simulation results, L = 10 mm.

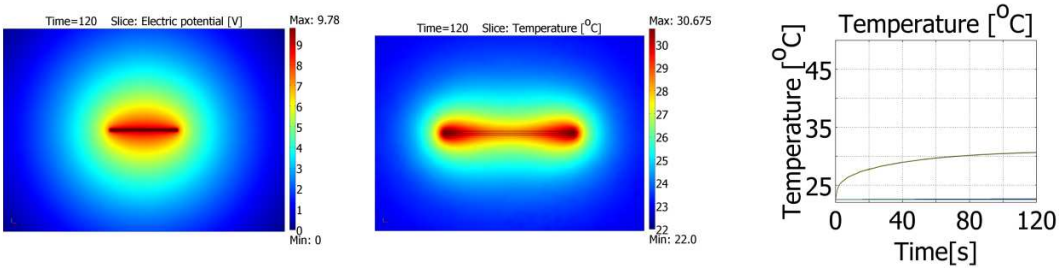

Figure 5.30 Applicator simulation results, L = 15 mm.

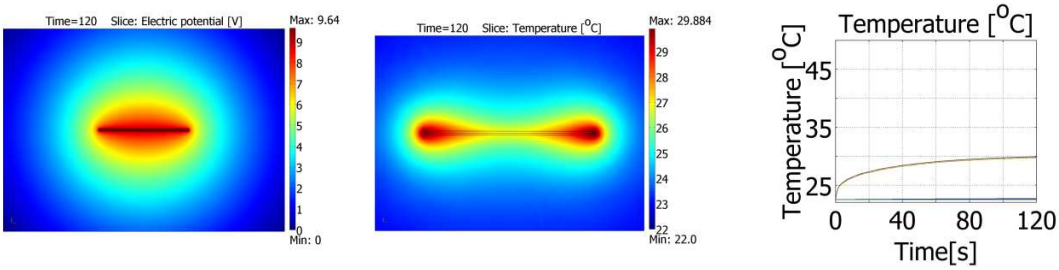

Figure 5.31 Applicator simulation results, L = 20 mm.

The temperature distributions in the simulations generally match with the corresponding experimental results. However, for the longer applicators (15 mm and 20 mm), the measured temperature distributions do not always show the typical “Q-tip” pattern observed with the simulations: the maximum temperature area is more extended at the distal end of the applicator than at the injection point. This can be attributed to the dielectric part of the experimental catheter that was not included in the model and which can both decrease the current density near the injection point, and increase thermal conduction away from the tissue. Also, steady state is

reached after 2 minutes in the computer simulations, but at 10 minutes in the experiments, probably because of the cooling effects of the air surrounding the set-up which was not accounted for in the models.

5.8 Applicator-in-Coil Experiments and Corresponding Simulations

In the coil embolization process, platinum coils are placed into the aneurysm and they can affect the steel applicator efficacy, thus in order to investigate its influence, a platinum coil was placed around the stainless steel applicator and the same parameters were monitored in the usual experimental set-up. The results and images of both experiments and computer simulations are shown in the following figures.

Table 5.5 Electrical and temperatures measurements for different lengths of an applicator placed in the middle of a coil.

Length (mm)	A (V)	B (V)	I (A)	P (W)	Z (ohm)	t (min)	Tbase °C	Tmax °C
3	14.4	1.32	0.066	0.86	198.2	2	22.5	25
3	14.6	1.32	0.066	0.88	201.2	5	22.5	27
3	14.4	1.32	0.066	0.86	198.2	10	22.5	27.9
6	13.6	1.54	0.077	0.93	156.6	2	22.5	24.8
6	13.7	1.52	0.076	0.93	160.3	5	22.5	25.2
6	13.6	1.52	0.076	0.92	158.9	10	22.5	26.1
10	12.5	1.84	0.092	0.98	115.9	2	22.5	24.6
10	12.5	1.82	0.091	0.97	117.4	5	22.5	25.1
10	12.7	1.84	0.092	1.00	118.0	10	22.5	25.9
15	12.5	1.86	0.093	0.99	114.4	2	22.5	24.5
15	12.3	1.9	0.095	0.99	109.5	5	22.5	25.1
15	12.2	1.94	0.097	1.00	105.8	10	22.5	25.6
20	12.4	1.92	0.096	1.01	109.2	2	22.5	23.6
20	12.6	1.86	0.093	1.00	115.5	5	22.5	23.9
20	12.2	1.91	0.0955	0.98	107.7	10	22.5	24.3

Figure 5.32 L = 3 mm, images taken after 2, 5 and 10 minutes of RF delivery

Figure 5.33 L = 6 mm, images taken after 2, 5 and 10 minutes of RF delivery

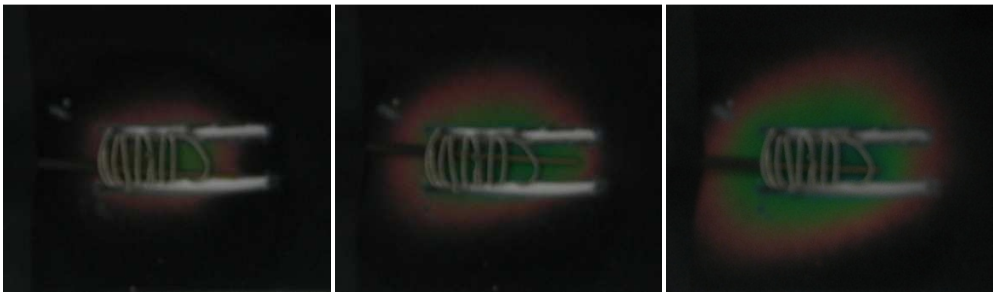

Figure 5.34 L = 10 mm, images taken after 2, 5 and 10 minutes of RF delivery

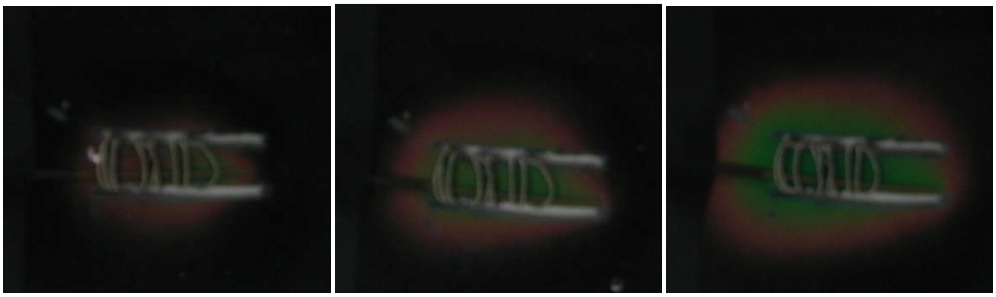

Figure 5.35 L = 15 mm, images taken after 2, 5 and 10 minutes of RF delivery

Figure 5.36 L = 20 mm, images taken after 2, 5 and 10 minutes of RF delivery

The following figures obtained from computer simulations prove that, same as the previous study, the temperature distributions in computer simulation satisfies the experimental results, however the maximum temperature is not always matched due to the lack of accurate measuring instruments.

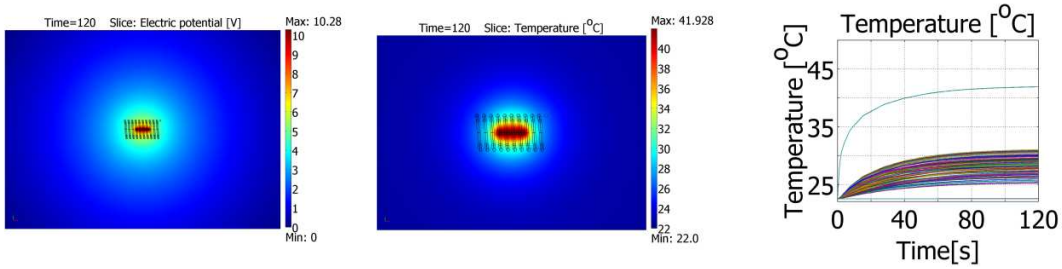

Figure 5.37 Applicator-in-coil simulations, L = 3 mm.

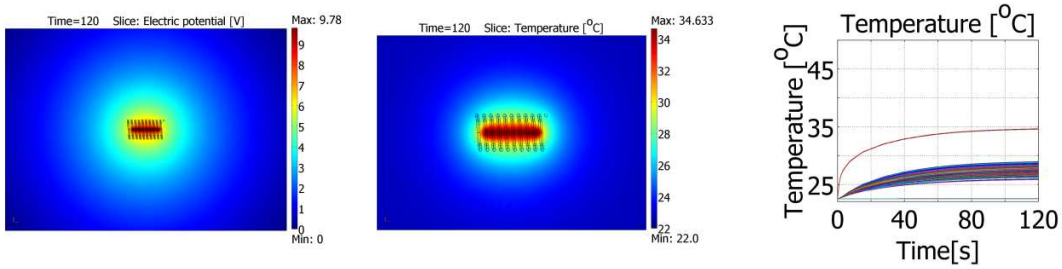

Figure 5.38 Applicator-in-coil simulations, L = 6 mm.

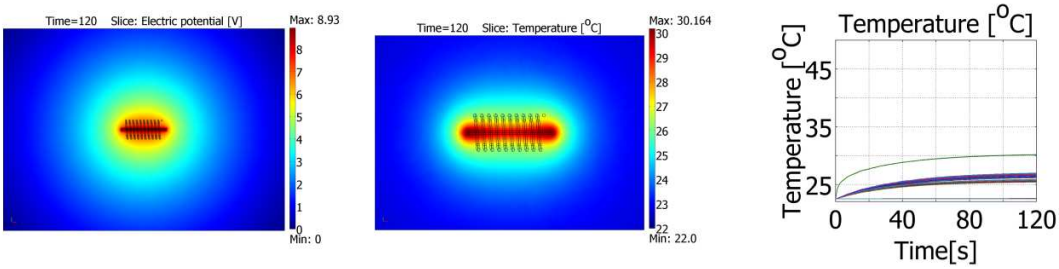

Figure 5.39 Applicator-in-coil simulations, L = 10 mm.

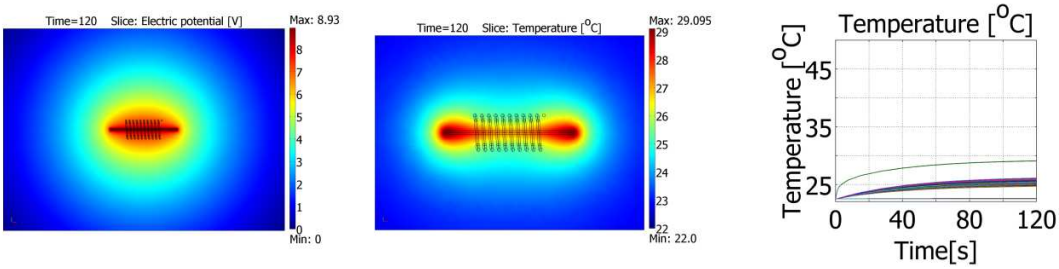

Figure 5.40 Applicator-in-coil simulations, L = 15 mm.

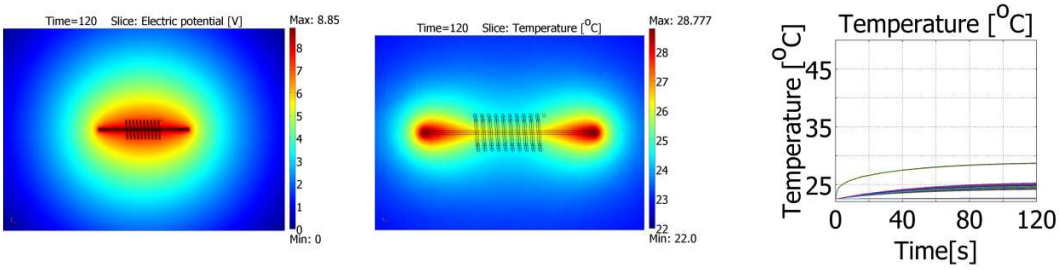

Figure 5.41 Applicator-in-coil simulations, L = 20 mm.

Again, the temperature distributions in the simulations generally match with the corresponding experimental results. However, for the longer applicators (15 mm and 20 mm), the measured temperature distributions do not always show the typical “Q-tip” pattern observed with the simulations: the maximum temperature area is more circular. This can be attributed to the thermal conduction of the coil which tends to be isothermal. Also, steady state is reached after 2 minutes

in the computer simulations, but at 10 minutes in the experiments, probably because of the cooling effects of the air surrounding the set-up that as not accounted for in the models.

5.9 Applicator-in-Brain Simulations

After having performed simulations and experiments to find the optimum parameters of RF application, it was time to simulate a model with characteristics more similar to those of the brain. Thus, a model (described in previous chapter) was made and various voltages were applied to one end of the stainless steel applicator for 120 seconds. The applicator model was created for two different lengths: 6 mm and 10 mm.

The following figures show the voltage distribution, the steady state temperature distribution and the temperature rise with time (from left to right) for both 6 mm and 10 mm long applicators while applying 5 V, 10 V and 15 V respectively.

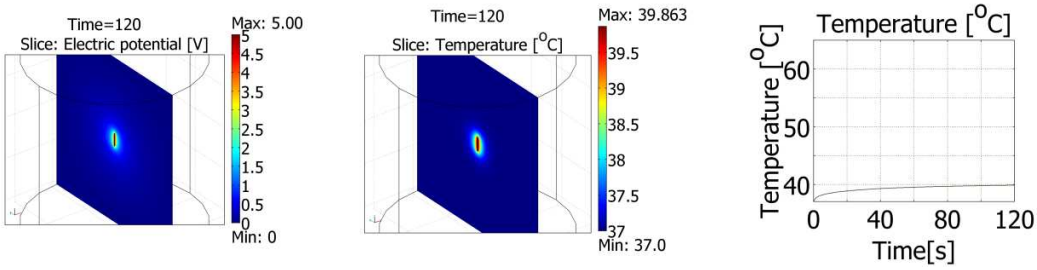

Figure 5.42 Brain model with 6 mm long applicator, voltage = 5 V.

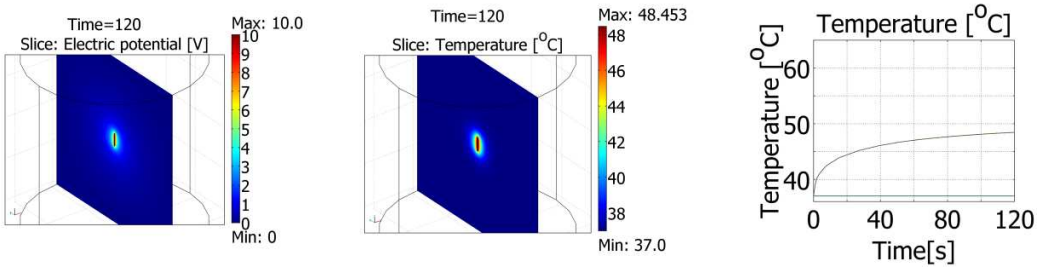

Figure 5.43 Brain model with 6 mm long applicator, voltage = 10 V.

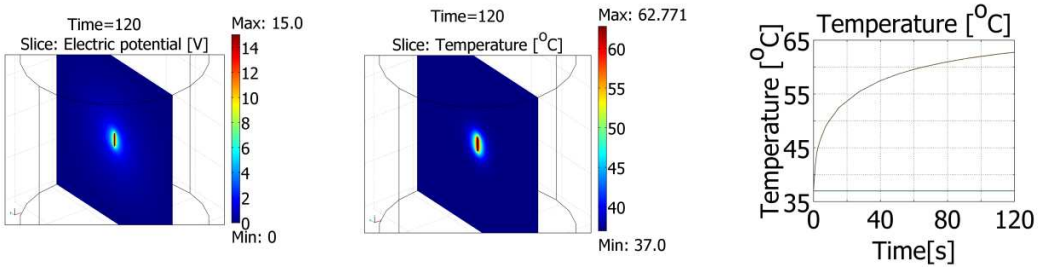

Figure 5.44 Brain model with 6 mm long applicator, voltage = 15 V.

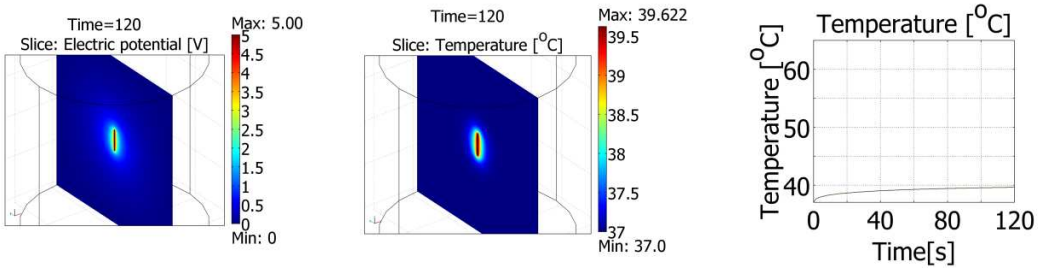

Figure 5.45 Brain model with 10 mm long applicator, voltage = 5 V.

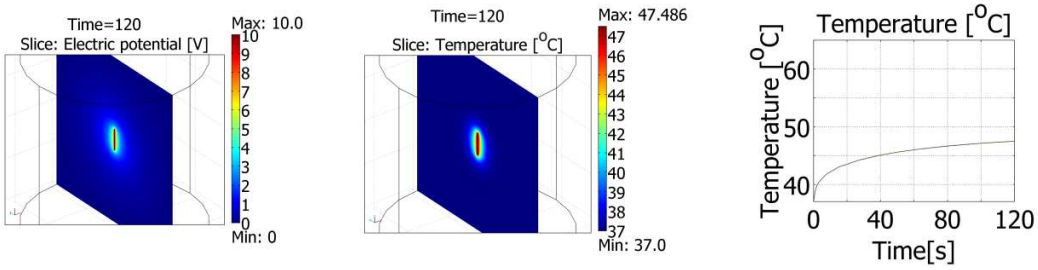

Figure 5.46 Brain model with 10 mm long applicator, voltage = 10 V.

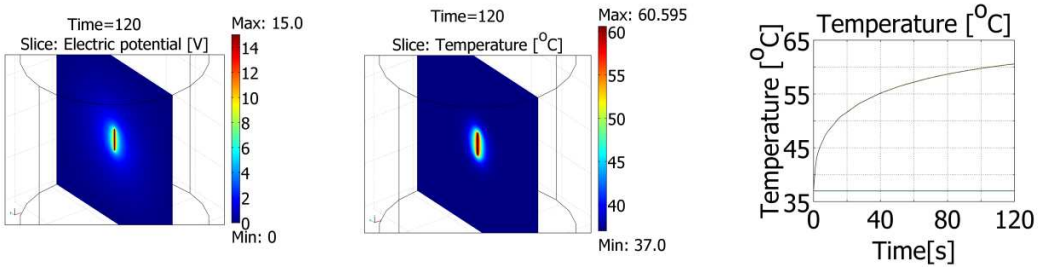

Figure 5.47 Brain model with 10 mm long applicator, voltage = 15 V.

According to a study in rat brain it was found that in a normal rat brain the temperature is decreased by 10 degree 5 mm away from the implant while performing hyperthermia (T. Kobayashi et al., 1986). Since the critical temperature for the spinal cord in mouse tissue for 2 minutes application is around 45-46°C (Dewhirst et al., 2003), in order to minimize the damage to the nervous tissue in the brain we have to take into account the duration of application and the applied voltage and also the type of the tissue. As it is seen in these pictures and considering that the critical temperature for the brain is 46°C after 2 minutes of application it is better to limit the applied voltage to 10 V and make sure that the duration of application does not exceed 120 seconds. So in this case the temperature would reach 48°C.

5.10 Temperature Dependant Electrical Conductivity

In order to study the effects of temperature dependant electrical conductivity, the applicator-in-brain model was solved while the local electrical conductivity was increased as the local temperature increased. This effect was studied in the models used in the previous section while applying different voltages of 5, 10 and 15 V. The results of this study are presented in the following figures which show the potential and the steady state temperature distributions as well as the electrical conductivity at the site which had the maximum temperature rise (and maximum conductivity change).

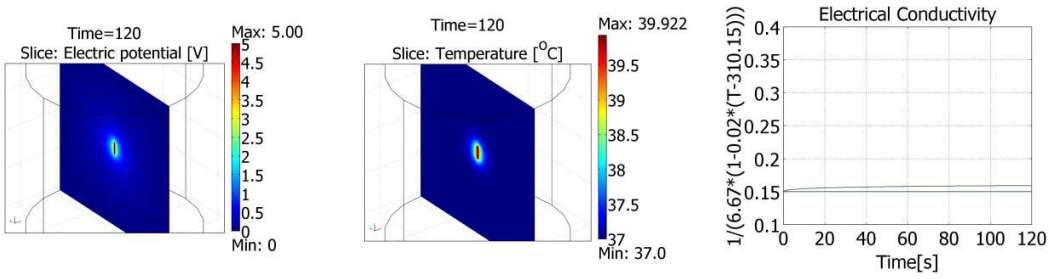

Figure 5.48 Temperature dependant brain model for a 6 mm long applicator at 5 V.

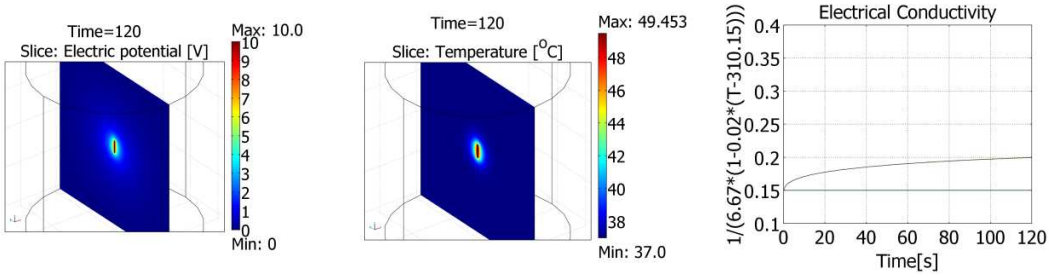

Figure 5.49 Temperature dependant brain model for a 6 mm long applicator at 10 V.

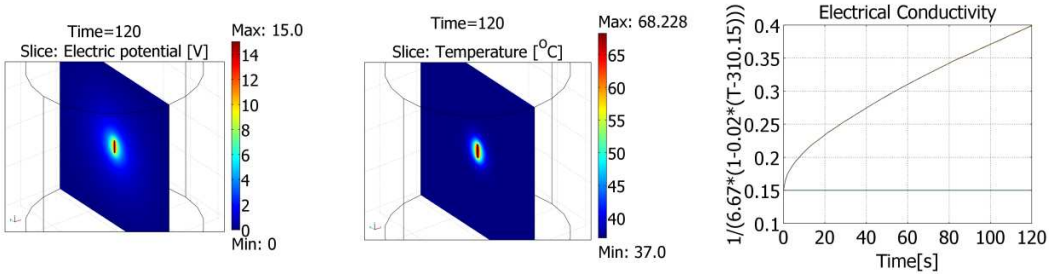

Figure 5.50 Temperature dependant brain model for a 6 mm long applicator at 15 V.

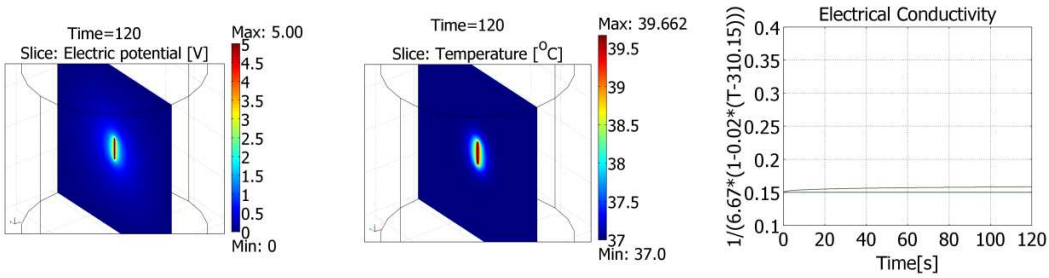

Figure 5.51 Temperature dependant brain model for a 10 mm long applicator at 5 V.

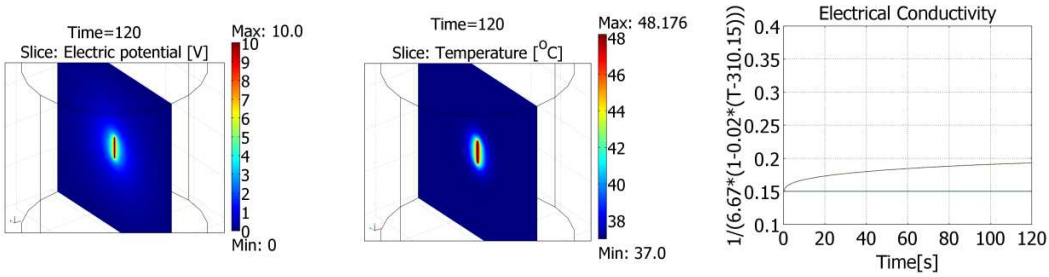

Figure 5.52 Temperature dependant brain model for a 10 mm long applicator at 10 V.

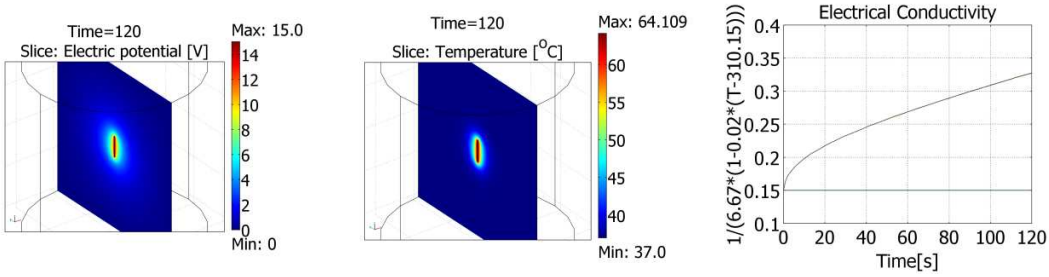

Figure 5.53 Temperature dependant brain model for a 10 mm long applicator at 15 V.

This study showed that for the lower voltages, where the temperature does not have a great rise, the influence of electrical conductivity change can be neglected. However, for applied voltages around 15 V or more, this effect cannot be neglected and it must be considered.

MAIN CONCLUSIONS

The present study was intended to investigate the technical modalities of radiofrequency ablation as an adjunct approach to prevent the recanalization around the embolized coils used for the treatment of cerebral aneurysms. We performed both *in vitro* experiments and computer simulations to investigate the mechanisms and the effects of radiofrequency current applied to an imbedded electrode (platinum coil or applicator) on the temperature distribution of surrounding tissue in order to optimize the radiofrequency parameters. All the computer simulations were validated with *in vitro* experiments which were done in a similar tissue phantom.

The following factors were found to have an important effect on the temperature distribution: electrode size and material, duration of energy delivery and applied power. The frequency of the current had no effect in the frequency band of 50 to 5000 kHz when the current was injected directly to a platinum coil and we concluded that we can neglect the inductance of the coil.

Experiments and simulations showed that the potential and temperature distribution along a simple platinum coil is not uniform when current is injected directly at the end of the coil. After measuring the impedance of different types of coils, we concluded that this effect is due to the large resistance of the coils (typically 400 Ω).

This finding suggested us to apply radiofrequency current through a low resistance applicator, and not directly to the platinum coil. We studied the effects of the size of this applicator and we conclude that an applicator with a length of 6 to 10 mm is appropriate to generate a uniform temperature distribution. Based on further modeling and experimental results, we also conclude that when radiofrequency current is injected into a steel applicator placed in the center of the endovascular coils, the presence of the coils do not alter significantly the temperature distribution.

The last computer simulations were done in models having a geometry closer to that of the brain. These models showed that the applied voltage should be around 10 V and the application duration should not exceed 120 second.

The effects of the mesh size for the finite element models and of the temperature dependence of the electrical conductivity of the tissue were also investigated to confirm the validity of our simulation results.

Our study has some limitations. We tried our best to make the computer models as similar as possible to the *in vitro* model; however, some factors such as cooling effects of the surrounding air, stability of the model, presence of the catheter shaft at the end of the applicator and accuracy of the measuring instruments were not taken into consideration. Another effect that was neglected in both *in vitro* and computer models was the shape of the coil. When an endovascular coil is placed in an aneurysm, it will lose its symmetrical shape and it will be deformed into a shapeless mass. Thus, the applicator will be placed within this mass and it will touch it, while in our models, we assumed that the endovascular coil has a symmetrical shape and that the applicator is placed exactly in the middle of the endovascular coil.

Finally, our results show the feasibility of producing very localized and well controlled heating patterns around endovascular coils with radiofrequency current. Further work could be performed to document in animal models the feasibility of using radiofrequency ablation for endothelial denudation and for the prevention of recanalization of embolized coils. Further work could also be pursued to investigate the possibility of heating aneurysms treated with a combination of flow diverter (stent) and coil that has been recently proposed for the treatment of wide necked aneurysms (Lylyk et al., 2010).

REFERENCES

Aburano, H., Kawamori, Y., Horiti, Y., Kitagawa, K., Sanada, J. & Matsui, O. (2006) Bronchial Artery Aneurysm Embolization with NBCA. CardioVascular and Interventional Radiology, 29 (6), pp.1141-1143.

Añon, V.V., Aymard, A., Gobin, Y.P., Casasco, A., Rüffenacht, D., Khayata, M.H., Abizanda, E., Redondo, A. & Merland, J.J. (1992) Balloon occlusion of the internal carotid artery in 40 cases of giant intracavernous aneurysm: technical aspects, cerebral monitoring, and results. Neuroradiology, 34 (3), pp.245-251.

Bendszus, M., Bartsch, A.J. & Solymosi, L. (2007) Endovascular Occlusion of Aneurysms Using a New Bioactive Coil: A Matched Pair Analysis With Bare Platinum Coils. Stroke, 38 (10), pp.2855-2857.

Brisman, J.L. (2009) Cerebral Aneurysm: Multimedia - eMedicine Neurosurgery. Available from: <http://emedicine.medscape.com/article/252142-media> [Accessed 27 July 2010].

Britz, G.W., Salem, L., Newell, D.W., Eskridge, J. & Flum, D.R. (2004) Impact of Surgical Clipping on Survival in Unruptured and Ruptured Cerebral Aneurysms: A Population-Based Study. Stroke, 35 (6), pp.1399-1403.

Brown, N. (1991) A mathematical model for the formation of cerebral aneurysms. Stroke; a Journal of Cerebral Circulation, 22 (5), pp.619-625.

Campi, A., Ramzi, N., Molyneux, A.J., Summers, P.E., Kerr, R.S., Sneade, M., Yarnold, J.A., Rischmiller, J. & Byrne, J.V. (2007) Retreatment of Ruptured Cerebral Aneurysms in Patients Randomized by Coiling or Clipping in the International Subarachnoid Aneurysm Trial (ISAT). Stroke, 38 (5), pp.1538-1544.

Darsaut, T., Bouzeghrane, F., Salazkin, I., Lerouge, S., Soulez, G., Gevry, G. & Raymond, J. (2007) The effects of stenting and endothelial denudation on aneurysm and branch occlusion in experimental aneurysm models. Journal of Vascular Surgery, 45 (6), pp.1228-1235.

Dewhirst, M.W., Viglianti, B.L., Lora-Michiels, M., Hanson, M. & Hoopes, P.J. (2003) Basic principles of thermal dosimetry and thermal thresholds for tissue damage from hyperthermia. International Journal of Hyperthermia: The Official Journal of European Society for Hyperthermic Oncology, North American Hyperthermia Group, 19 (3), pp.267-294.

Ferrito, G., Quilici, N., Gianni, G., Prosetti, D., Scazzeri, F. & Marcacci, G. (1994) Balloon

occlusion of the carotid artery in the treatment of cavernous giant aneurysms: two cases. The Italian Journal of Neurological Sciences, 15 (8), pp.423-427.

Guglielmi, G. (1998) Use of the GDC crescent for embolization of tumors fed by cavernous and petrous branches of the internal carotid artery. Journal of Neurosurgery, 89 (5), pp.857-860.

Guglielmi, G., Viñuela, F., Sepetka, I. & Macellari, V. (1991) Electrothrombosis of saccular aneurysms via endovascular approach. Journal of Neurosurgery, 75 (1), pp.1-7.

Iijima, A., Piotin, M., Mounayer, C., Spelle, L., Weill, A. & Moret, J. (2005) Endovascular Treatment with Coils of 149 Middle Cerebral Artery Berry Aneurysms1. Radiology, 237 (2), pp.611-619.

Kaouk, Z., Shahidi, A., Savard, P. & Molin, F. (1996) Modelling of myocardial temperature distribution during radio-frequency ablation. Medical and Biological Engineering and Computing, 34 (2), pp.165-170.

Kawanabe, Y., Sadato, A., Taki, W. & Hashimoto, N. (2001) Endovascular Occlusion of Intracranial Aneurysms with Guglielmi Detachable Coils: Correlation Between Coil Packing Density and Coil Compaction. Acta Neurochirurgica, 143 (5), pp.451-455.

Kobayashi, T., Kida, Y., Tanaka, T., Kageyama, N., Kobayashi, H. & Amemiya, Y. (1986) Magnetic induction hyperthermia for brain tumor using ferromagnetic implant with low Curie temperature. Journal of Neuro-Oncology, 4 (2), pp.175-181.

Lempert, T.E., Malek, A.M., Halbach, V.V., Phatouros, C.C., Meyers, P.M., Dowd, C.F. & Higashida, R.T. (2000) Endovascular Treatment of Ruptured Posterior Circulation Cerebral Aneurysms : Clinical and Angiographic Outcomes. Stroke, 31 (1), pp.100-110.

Liebeskind, D.S. (2009) Cerebral Aneurysms: eMedicine Neurology. Available from: <http://emedicine.medscape.com/article/1161518-overview> [Accessed 29 July 2010].

Linfante, I. & Wakhloo, A.K. (2007) Brain Aneurysms and Arteriovenous Malformations: Advancements and Emerging Treatments in Endovascular Embolization. Stroke, 38 (4), pp.1411-1417.

Lozier, A.P., Connolly, E.S., Lavine, S.D. & Solomon, R.A. (2002) Guglielmi Detachable Coil Embolization of Posterior Circulation Aneurysms: A Systematic Review of the Literature. Stroke, 33 (10), pp.2509-2518.

Lylyk, P., Pabon, B., Ferrario, A., Scrivano, E., Lundquist, J., Ceratto, R. & Nella, R. (2010)

Endovascular Treatment of Ruptured Intracranial Aneurysms with Pipeline™ Flow-Diverter Stent: Pros and Cons. Available from: <http://www.aans.org/Education%20and%20Meetings/Annual%20Meetings/~/Media/Files/Education%20and%20Meetingf/Annual%20Meeting/2010/pdfs/OralPapersForWeb.ashx>.

McDougall, C.G., Halbach, V.V., Dowd, C.F., Higashida, R.T., Larsen, D.W. & Hieshima, G.B. (1998) Causes and management of aneurysmal hemorrhage occurring during embolization with Guglielmi detachable coils. Journal of Neurosurgery, 89 (1), pp.87-92.

Meyers, P.M., Thakur, G.A. & Tomsick, T.A. (1999) Temporary Endovascular Balloon Occlusion of the Internal Carotid Artery with a Nondetachable Silicone Balloon Catheter: Analysis of Technique and Cost. AJNR Am J Neuroradiol, 20 (4), pp.559-564.

Molyneux, A.J., Kerr, R.S.C., Birks, J., Ramzi, N., Yarnold, J., Sneade, M. & Rischmiller, J. (2009) Risk of recurrent subarachnoid haemorrhage, death, or dependence and standardised mortality ratios after clipping or coiling of an intracranial aneurysm in the International Subarachnoid Aneurysm Trial (ISAT): long-term follow-up. Lancet Neurology, 8 (5), pp.427-433.

Murayama, Y., Vinuela, F., Tateshima, S., Gonzalez, N.R., Song, J.K., Mahdavieh, H. & Iruela-Arispe, L. (2002) Cellular Responses of Bioabsorbable Polymeric Material and Guglielmi Detachable Coil in Experimental Aneurysms. Stroke, 33 (4), pp.1120-1128.

Murayama, Y., Viñuela, F., Duckwiler, G.R., Gobin, Y.P. & Guglielmi, G. (1999) Embolization of incidental cerebral aneurysms by using the Guglielmi detachable coil system. Journal of Neurosurgery, 90 (2), pp.207-214.

Ng, P., Khangure, M., Phatouros, C., Bynevelt, M., ApSimon, H. & McAuliffe, W. (2002) Endovascular Treatment of Intracranial Aneurysms With Guglielmi Detachable Coils: Analysis of Midterm Angiographic and Clinical Outcomes. Stroke, 33 (1), pp.210-217.

Nishi, S., Taki, W., Nakahara, I., Yamashita, K., Sadatoh, A., Kikuchi, H., Hondo, H., Matsumoto, K., Iwata, H. & Shimada, Y. (1996) Embolization of cerebral aneurysms with a liquid embolus, EVAL mixture: Report of three cases. Acta Neurochirurgica, 138 (3), pp.294-300.

Raymond, J., Darsaut, T., Salazkin, I., Gevry, G. & Bouzeghrane, F. (2008) Mechanisms of Occlusion and Recanalization in Canine Carotid Bifurcation Aneurysms Embolized with Platinum Coils: An Alternative Concept. AJNR Am J Neuroradiol, 29 (4), pp.745-752.

Raymond, J., Guilbert, F., Metcalfe, A., Gevry, G., Salazkin, I. & Robledo, O. (2004) Role of the

Endothelial Lining in Recurrences After Coil Embolization: Prevention of Recanalization by Endothelial Denudation. Stroke, 35 (6), pp.1471-1475.

Raymond, J., Guilbert, F., Weill, A., Georganos, S.A., Juravsky, L., Lambert, A., Lamoureux, J., Chagnon, M. & Roy, D. (2003) Long-Term Angiographic Recurrences After Selective Endovascular Treatment of Aneurysms With Detachable Coils. Stroke, 34 (6), pp.1398-1403.

Raymond, J., Leblanc, P., Desfaits, A., Salazkin, I., Morel, F., Janicki, C. & Roorda, S. (2002) In Situ Beta Radiation to Prevent Recanalization After Coil Embolization of Cerebral Aneurysms. Stroke, 33 (2), pp.421-427.

Raymond, J., Leblanc, P., Morel, F., Salazkin, I., Gevry, G. & Roorda, S. (2003) Beta Radiation and Inhibition of Recanalization After Coil Embolization of Canine Arteries and Experimental Aneurysms: How Should Radiation Be Delivered? Stroke, 34 (5), pp.1262-1268.

Raymond, J., Metcalfe, A., Salazkin, I., Gevry, G. & Guilbert, F. (2006) Endoluminal Cryotherapy to Prevent Recanalization after Endovascular Occlusion with Platinum Coils. Journal of Vascular and Interventional Radiology, 17 (9), pp.1499-1504.

Raymond, J., Mounayer, C., Salazkin, I., Metcalfe, A., Gevry, G., Janicki, C., Roorda, S. & Leblanc, P. (2006) Safety and Effectiveness of Radioactive Coil Embolization of Aneurysms: Effects of Radiation on Recanalization, Clot Organization, Neointima Formation, and Surrounding Nerves in Experimental Models. Stroke, 37 (8), pp.2147-2152.

Raymond, J., Savard, P., Salazkin, I. & Bouzeghrane, F. (2010) Radiofrequency endothelial ablation prevents recanalization after endovascular coil occlusion: in vitro and in vivo assessment. Journal of Vascular and Interventional Radiology: JVIR, 21 (1), pp.101-107.

Raymond, J., Silvaggio, J., Guilbert, F., Weill, A. & Roy, D. (2005) Impact of surgical treatment of unruptured aneurysms. Stroke; a Journal of Cerebral Circulation, 36 (10), pp.2069-2070.

Sadato, A., Taki, W., Ikada, Y., Nakahara, I., Matsumoto, K., Tanaka, M. & Kikuchi, H. (1995) Immediately detachable coil for aneurysm treatment. AJNR Am J Neuroradiol, 16 (7), pp.1459-1462.

Schievink, W.I. (1997) Intracranial Aneurysms. N Engl J Med, 336 (1), pp.28-40.

Shimko, N., Savard, P. & Shah, K. (2000) Radio frequency perforation of cardiac tissue:

modelling and experimental results. Medical & Biological Engineering & Computing, 38 (5), pp.575-582.

Shojima, M., Oshima, M., Takagi, K., Torii, R., Hayakawa, M., Katada, K., Morita, A. & Kirino, T. (2004) Magnitude and Role of Wall Shear Stress on Cerebral Aneurysm: Computational Fluid Dynamic Study of 20 Middle Cerebral Artery Aneurysms. Stroke, 35 (11), pp.2500-2505.

Shojima, M., Oshima, M., Takagi, K., Torii, R., Nagata, K., Shirouzu, I., Morita, A. & Kirino, T. (2005) Role of the Bloodstream Impacting Force and the Local Pressure Elevation in the Rupture of Cerebral Aneurysms. Stroke, 36 (9), pp.1933-1938.

Standhardt, H., Boecher-Schwarz, H., Gruber, A., Benesch, T., Knosp, E. & Bavinzski, G. (2008) Endovascular Treatment of Unruptured Intracranial Aneurysms With Guglielmi Detachable Coils: Short- and Long-Term Results of a Single-Centre Series. Stroke, 39 (3), pp.899-904.

Taschner, C.A., Leclerc, X., Rachdi, H., Barros, A.M. & Pruvo, J. (2005) Matrix Detachable Coils for the Endovascular Treatment of Intracranial Aneurysms: Analysis of Early Angiographic and Clinical Outcomes. Stroke, 36 (10), pp.2176-2180.

Taylor, C.L., Yuan, Z., Selman, W.R., Ratcheson, R.A. & Rimm, A.A. (1995) Cerebral arterial aneurysm formation and rupture in 20,767 elderly patients: hypertension and other risk factors. Journal of Neurosurgery, 83 (5), pp.812-819.

Tsutsumi, K., Ueki, K., Usui, M., Kwak, S. & Kirino, T. (1999) Risk of Subarachnoid Hemorrhage After Surgical Treatment of Unruptured Cerebral Aneurysms. Stroke, 30 (6), pp.1181-1184.

University of Virginia Health Center (2007) Cerebral Aneurysm — University of Virginia Health System [Internet]. Available from: <http://uvahealth.com/services/neurosciences/conditions-and-treatments/cerebral-aneurysm/?searchterm=coil%20embolization%20for%20cerebral%20aneurysm> [Accessed 29 July 2010].

Vanninen, R. & Manninen, I. (2007) Onyx, a New Liquid Embolic Material for Peripheral Interventions: Preliminary Experience in Aneurysm, Pseudoaneurysm, and Pulmonary Arteriovenous Malformation Embolization. CardioVascular and Interventional Radiology, 30 (2), pp.196-200.

White, J., Ken, C., Cloft, H. & Kallmes, D. (2008) Coils in a Nutshell: A Review of Coil Physical Properties. AJNR Am J Neuroradiol, 29 (7), pp.1242-1246.

Wiebers, D.O., Whisnant, J.P., Huston, J., Meissner, I., Brown, R.D., Piepgras, D.G., Forbes, G.S., Thielen, K., Nichols, D., O'Fallon, W.M., Peacock, J., Jaeger, L., Kassell, N.F., Kongable-Beckman, G.L. & Torner, J.C. (2003) Unruptured intracranial aneurysms: natural history, clinical outcome, and risks of surgical and endovascular treatment. Lancet, 362 (9378), pp.103-110.

Yale Medical Group (2010) Endovascular Coiling. Yale School of Medicine. Available from: <http://www.yalemedicalgroup.org/stw/Page.asp?PageID=STW029076>.

Zucchi, V., Narducci, P., Padolecchia, R., Guglielmi, G., Puglioli, M., Castagna, M., Nardini, V., Collavoli, P.L., Guidetti, G. & Dazzi, M. (2001) Role of Electrothrombosis in Aneurysm Treatment with Guglielmi Detachable Coils: An In Vitro Scanning Electron Microscopic Study. AJNR Am J Neuroradiol, 22 (9), pp.1757-1760.